Design of a Triboelectric Charge Measurement System

Design of a Triboelectric Charge Measurement System

By

Francesca Madan, B.Tech

A Thesis

Submitted to the School of Graduate Studies

In Partial Fulfillment of the Requirements

For the Degree of

Master of Applied Science

In Mechanical Engineering

McMaster University

Master of Applied Science (2023)
(Mechanical Engineering)

McMaster University
Hamilton, Ontario

TITLE: Design of a Triboelectric Charge Measurement System

AUTHOR: Francesca Madan
B. Tech (McMaster University

SUPERVISORS: Dr. Amin Rajabzadeh
Dr. Moein Mehrtash

NUMBER OF PAGES: i- 92

Abstract

Tribo-charging is the scientific phenomenon of particles collecting charge through frictional collisions. Disadvantages of tribocharging can occur during powder-handling operations, for instance particle deposition and adhesion. In more extreme cases when particles are excessively charged, electrostatic discharge may occur and cause fire or explosion hazards. With its negatives there are positives, as tribocharging is used in many industries such as the automotive, pharmaceutical, and waste management, coal, and food industry. Research would be beneficial in understanding how the powders perform in operational settings, such as the blending and separation processes. The chemical and physical properties play a key role in affecting the manufacture process and final product. Understanding the chemical or physical composition of the different particles can result in a more effective process.

Methods for collecting this charge are a Faraday cup, on-line current measurement, Electric Low-Pressure Impactor (ELPI), and Electronic Single Particle Relaxation Time (ESPART). Research articles have predominately been completed with measurement research using the Faraday cup. Factors that can affect the charging are humidity, work function, particle size, and particle morphology. This project aims to analyze the physical and chemical composition of food-grade powders by creating a system that will transport particles consistently and reliably through a tube to have the charge created by tribo-charging accurately measured. Once the charge is collected, external factors affecting the charge are to be compared and analyzed based off the ratio or compositional make-up of the powder.

The goal can be achieved by creating an offline charge measurement system and pairing it with a consistent mass delivery system. Meaning the mass and charge are measured at the

beginning and end of the process, not in real-time. Two mass delivery and one charge measurement systems for online measurement were designed and constructed, and one design for both mass delivery and charge measurement for an offline system were designed and constructed. Online measurement means that real-time data for the charge and mass are being collected to obtain the charge-mass ratio at that exact time frame. The mass delivery designs are as followed:

- 1st Design: Screw feeder and vibrator hybrid to create consistent flow rate and no "clumping" of materials. However, the design proved to have fluctuations within the mass, and the contact of the Faraday cup with the exit tubing caused the powder delivery to have extra forces that skewed the mass measurements.
- 2nd Design: A fluidized bed was utilized in tandem with vibrator, however external and internal factors like mass of powder, air flow resistance, and location of powder within the bed caused a flowrate that was able to increase, but not at a consistent rate.

The first charge measurement system was planned to be an online charge measurement using an electrometer and the Faraday cup as a verification method for results. However, the charge measured did not match the mass in relation to time. This could have been due to charged particles escaping the Faraday cup and coating the charged tube – essentially grounding it and stopping any further measurements from being completed. In addition, incorrect grounding of the system caused the charge to flow towards any unground section of the system. This caused no charge measurement and the danger of having a charge lingering on the system. Finally, electrical issues were caused by the loose charged powder that escaped the Faraday cup and came into contact with any of the electrical equipment

within range. The offline charge measurement is comprised solely of the Faraday cup connected to an electrometer. The third mass delivery offline design, utilizing the fluidized bed, is being implemented and the offline charge measurement system is also in use. Each section of the charge measurement and mass delivery is contained to prevent further electrical damage of equipment.

Trail runs for comparison of dried/undried pure powders, mixture ratio of combination powders, airflow, sifted particle size, and protein content have been completed to analyze the effect these factors have on the charge-mass ratio of the powders. Looking at the experiments, it can be seen that dried pure powders have a higher charge-mass ratio than undried pure powders. Further the sifted size ranges show smaller particle sizes obtain greater charge-mass ratios. While the powder mixtures should show directly proportional charge-mass ratios to the ratio of powders mixed it, this is not the case due to total mass accumulated at the end of the system. However, protein content testing resulted in showing accurate representation of the ratios mixed for each powder. Therefore, hypothesis for the non-linear relationship could be due to the aggregation or coagulation of the two pure powders. Airflow was analyzed from 5-20 LPM and the mass-charge ratio was collected, the results showed an increase in overall mass-charge ratio, but at both 10 and 20 LPM there were “drops” or decrease in charge. The reason for the charge-mass ratio increase can be attributed to the impact force and the decrease in charge-mass ratio can be attributed to the laminar or turbulent phase of airflow. Finally, protein content results indicated that as the wt% increases, the charge-mass ratio also increased, with the exception of chickpea flour. It was hypothesized that both particle shape and size played key roles in effecting the charge-mass ratio of chickpea flour, using SEM photos both size distribution of the particles and

shape of particles were analyzed. Results indicated that the particle size was within the range, but the shape of the chickpea flour was spherical which can cause better fluidization. Therefore, it was determined that the shape or morphology of the particles played a more influential role in changing the charge-mass ratio of the particle, causing it to be an outlier.

Mathematical modelling, using Matsuda's tribocharging model based on repeated particle impacts on the wall was used to determine the effect of the work function for the particles. It was concluded that the charge-mass ratio and contact potential difference increased in proportion to each other. This trend was also seen with the protein content of each powder and the contact potential difference. Analysis for the math modelling corresponded with the results in the real time experiments. Observing that the results were already anticipated, no new conclusions could be drawn from the math modeling.

Further research should be conducted to determine effects of humidity and acidity/basicity on tribo-charging and how it can be correlated with protein content results or other environmental factors. Specifically with acidity and basicity, tests to determine functional groups would need to be completed and the results correlated with charge and compared against other external factors such as protein content. In addition, for the math modeling, calculations to find the exact values for the mean collision numbers could lead to more accurate contact potential difference or work function values for the effect of particle charge.

Acknowledgment

First and foremost, I would like to thank my supervisors Amin Rajabzadeh and Moein Mehrtash. My supervisors always were available to assist me and always had a free moment to talk whenever I needed guidance. They took the time to constantly challenge and push me, which I am very thankful for. Without challenge and push, there wouldn't be any growth.

I would also like to thank George Apostol who was available to help me with manufacturing and design whenever I needed support. He was always available to hear my questions or ideas and would then help me produce something better than I had anticipated. Finally, I would like to thank Vivian Phung for performing the Bradford assay for protein content testing, and the Department of Mechanical Engineering.

Table of Contents

List of Figures

List of Tables

Chapter 1. Introduction

Tribo-charging is the scientific phenomenon when particles become electrostatically charged by contact friction (Matsusaka, Shuji, et al, 2010). This charge can occur by particles being pressed or rubbed. While this phenomenon does not require a certain form of solid, effects can most easily be seen with powder, prompting numerous research papers studying how charge created by tribo-charging affects the physical and chemical composition of particles in powder form.

Practical applications for tribo-charging can be seen through various industries. The pharmaceutical industry uses tribo-charging to research the properties of medicinal powders that are used in inhalers. The research is implemented for a better analysis of the chemical and physical characteristics of the powders being transported through the inhalers at the aerosolization stage (Karner & Urbanetz, 2013). Additionally, tribo-charging is used widely in separating materials, for example separating coal from other minerals or the separating of waste management. The materials are sent through tribo-charging mechanisms, for example down a metal ramp, and collect charge. The charged materials are then funneled into a contained unit with a cathode and anode on separate sides of the container. The materials will separate based on charge and move towards the magnet with opposite polarity, separating the different materials (Zhang, Guangwen, et al, 2013). A large portion of separation tribo-charging can be found within the food industry. The food industry uses tribocharging for the extraction of proteins, starch, and fibers. Electrostatic separation is a method used for dry fractionation of plant proteins or flours and is used for the production of protein-, starch- and fiber-enriched products (Assatory et. al, 2019). In the

automotive industry, tribo-charging is used to adhere paint or coatings to vehicles. Powders are made airborne as they are sent through tubing towards the nozzle, resulting in the particles receiving charge. The nozzle then sprays the charged particles on the surfaces that have been given an opposite polarity. This results in an even coating as the oppositely charged particles are attracted (Krämer, H., 1993). This process is also used within the furniture industry among others to apply powder coatings (Jocham et. al, 2011).

Regardless of all the positive implementations of the scientific phenomenon, tribo-charging has been seen in the past as a greater liability (Kramer, 1998). During powder-handling operations, particle deposition and adhesion can occur. The layers of additional charged particles on machinery can cause sparks or shocks throughout the systems, damaging equipment and possibly the people working on the machinery. In more extreme cases when particles are excessively charged, electrostatic discharge may occur and cause fire or explosion hazards (Kramer, 1993).

1.1. Objective

This research's goal is to create a system that will be able to transport particles consistently and reliably through a tube to have the charge accurately measured. Once the system is fully functioning, tests with varying food-grade powders are to be run. The objective is to compare the charge collected by the system to the compositional make-up of the powders that flow through. Simultaneously, tests for protein content will be conducted to get quantifiable results that can directly correlate to the charges produced by the powders.

The mass delivery and charge measurement of the system has been redesigned and manufactured. Initial testing using the pure powders have been completed. In addition to

the pure powder results, tests were completed to analyze the effect of airflow, particle size, protein content, and mixed powder ratios. Math modelling was completed to observe how the charge-mass ratio of different particle types affect the work function using quantifiable values.

1.1. Thesis Outline

This thesis is structured in the following approach. Section 1 is the introduction of the topic of tribo-charging, the objective and novelty of this report. Section 2 contains the literature review, where an in-depth look is provided for the methodology of research previously completed and the environmental factors that affect tribo-charging. Section 3 describes the methodology and iterations of design for both the mass delivery and charge measurement system. Section 4 contains results and discussions of the real time experiments completed to obtain mass-charge ratio using the different external factors. Math using the experimental charge values to estimate a property such as contact potential can be found in section 5. Section 6 contains my conclusions from the collective research completed within the whole report. Finally, section 7 contains the appendix where extra drawings such as the 2D/3D CAD models can be found.

Chapter 2. Literature Review

Tribo-charging is the scientific phenomenon where particles obtain a charge through contact such as rubbing or pushing, the particles become what is commonly known as becoming electrostatically charged (Matsusaka, Shuji, et al, 2010). During powder-handling operations, the charged particles can cause problems, for instance, particle deposition and adhesion. In more extreme cases when particles are excessively charged, electrostatic discharge may occur and cause fire or explosion hazards (Kramer, 1998 & 1993). However, even with some negative connotations surrounding triboelectric charging, many industries find a positive way to apply this phenomenon. Applications include pharmaceutical inhalers, powder coating, and material separation (Karner & Urbanetz, 2013, Zhang, Guangwen, et al. 2013, Krämer, H., 1993, & Jocham et. al, 2011). This literature review will discuss the particle physics for tribocharging and by what method the ions and electrons are reorganized to create the charges. In addition, the methodology used to measure the charge and some of the environmental factors that can affect and alter the charge will be examined.

2.1. Ion, Electron, and Material Transfer

Electron transfer is based on the contact potential difference due to work functions for metal-to-metal contacts. Work function can be defined as the minimum quantity of energy which is required to remove an electron from the surface of a given solid (Trigwell et. al, 2003). When metals are isolated electrically, the charge can be measured. This is generally due to the tribo-charging of metals going unnoticed from the conductivity of the material. Using equation 1, the contact potential difference, V_c (volts), can be determined with the

work functions of the two materials, ϕ_1 and ϕ_2 (electron volts), and the elementary charge (coulombs), e (Harper, 1951).

$$V_c = \frac{\phi_1 - \phi_2}{e} \quad (1)$$

The net charge is equal to the product of the contact potential difference and the capacitance between the two materials (C_o), as seen in equation 2.

$$\Delta q = C_o V_c \quad (2)$$

The charge from metal to insulator can be simulated using an "effective" work function being assigned to the insulator. The amount of transferred charge is determined to equalize the energy levels of the two materials, resulting in a different net charge equation then displayed in equation 3, where ϕ_i is the work function of the insulator and ϕ_m is the work function of the metal. The updated equation is as follows: (Matsusaka, Shuji, et al, 2010)

$$\Delta q = C_o \frac{-(\phi_i - \phi_{m)}}{e} \quad (3)$$

Initially, ion transfer caused by water absorption was believed to be a major factor of charge transfer. However, an analysis of the effect of water vapor was conducted, and research showed an increase in surface conductivity with a lowering of the electrical breakdown strength of air. This results in lower charge transfer and maximum potential within moist atmospheres (large water absorption), contradicting the initial belief (Lee, 1994). In more modern times, ion transfer has started to pick up traction once again and is being used within working industries. For example, the electrophotographic industry used charge control agents (consisting of mobile and immobile ions) to accelerate and control the charging

process (Matsusaka, Shuji, et al, 2010). Experiments using mass spectrometry and scanning probe microscopy are being used to observe ion transfer and its applications within tribo-charging (Mizes et. al, 1990 & Saurenbach et. al, 1992). Further experiments are needed to conduct thorough research into this specific charge transfer.

The impact and friction of insulator-to-metal, metal-metal, or insulator-insulator can cause a transfer of materials between the two surfaces. This can result in impurities or the transfer of contaminated materials. If the transferred material carries a charge – charge transfer will occur. (Tanoue et. al, 1999).

2.2. Methods of Charging

Modes of charging are contact charging, frictional charging, and induction charging, seen in figure 1. Contact charging occurs when two solids come into contact and then separate. At the point of contact, the difference between the solid energy levels results in electrostatic charge that will transfer between the two bodies until an equilibrium state is achieved. Once the solids are then separated, the equilibrium is demolished and two oppositely charged layers form on the surfaces of the solids (Moughrabiah et. al, 2009 & Yang, 1998). Frictional charging occurs when the two solids are rubbed together. The difference between contact (pressing) the solids together rather than rubbing them is hard to identify, therefore the term "tribo-electric charging" is widely used to describe both methods (Moughrabiah et. al, 2009 & Yang, 1998). Induction charging uses an already charged object brought close to an isolated object that is conductive and has a neutral charge. The polarity of the charged object can cause change in whether the electrons on the surface of the neutral object will either move closer or farther away. Grounding the neutrally charged object will result in the object

being positively or negatively charged (the charge will be opposite of the inducing charge source). Once the grounding and induced charged sources are removed, the neutral object will turn into a charged object with the opposite charge polarity of the induced charge source (Yang, 1998).

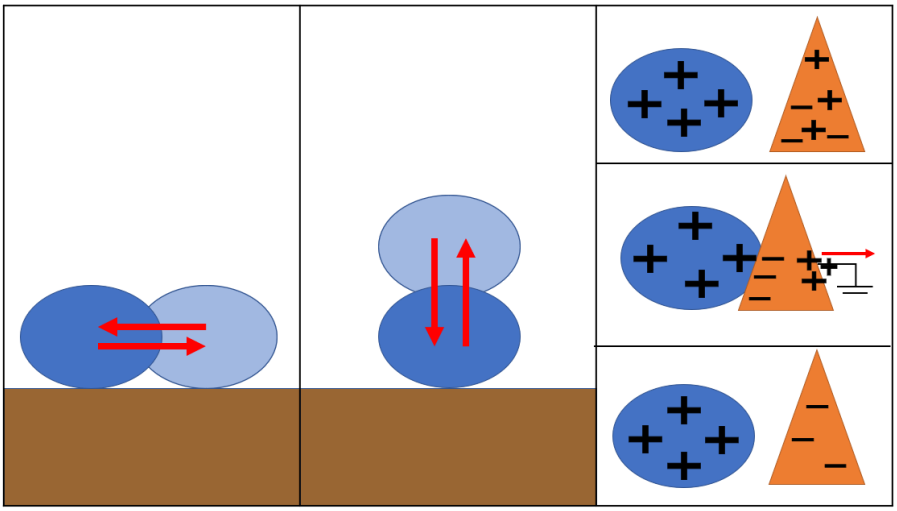

Figure 1 a-c. Diagram showing the different methods of charging: a) frictional charging, b) contact charging, and c) induction charging.

2.3. Real-Time Measuring Apparatus

The charge of the particles found during tribo-charging can be measured in real-time. Looking at research papers, there are four main methods to measure the charge. Table 1 displays various research papers collected using different measurement systems. In addition, with each paper, the results of the research in addition to external factors affecting the charge measurement have been noted.

A Faraday cup, seen in figure 2, or cage is two conductive cups or contained area (one inside of the other with insulation in between) that can measure the charge of the total amount of

particles contained in its boundaries. The inner cup is connected to an electrometer or coulombmeter and measures the charge by detecting the voltage generated across a known capacitor. When the material is placed inside the cup, the walls will collect an equal but opposite polarity charge due to induction charging. The outer cup is grounded and shields the inner cup from external electric fields and other noise (Mehrani, 2005). There are two types, open and closed. The "closed"-ended Faraday cup has a solid bottom, giving a place for the powder to remain after it has been transported. While this method gives a certainty that the powder will be able to have its charge measured, there is a risk of powder "escaping" the cage due to extra airflow and skewing results. The "open"-ended Faraday cup is the same device but missing the bottom (can run straight through). This gives the user the option to place the Faraday cup anywhere along their system line. This measuring device is widely used in research, as it is the uncomplicated set-up to receive a charge measurement.

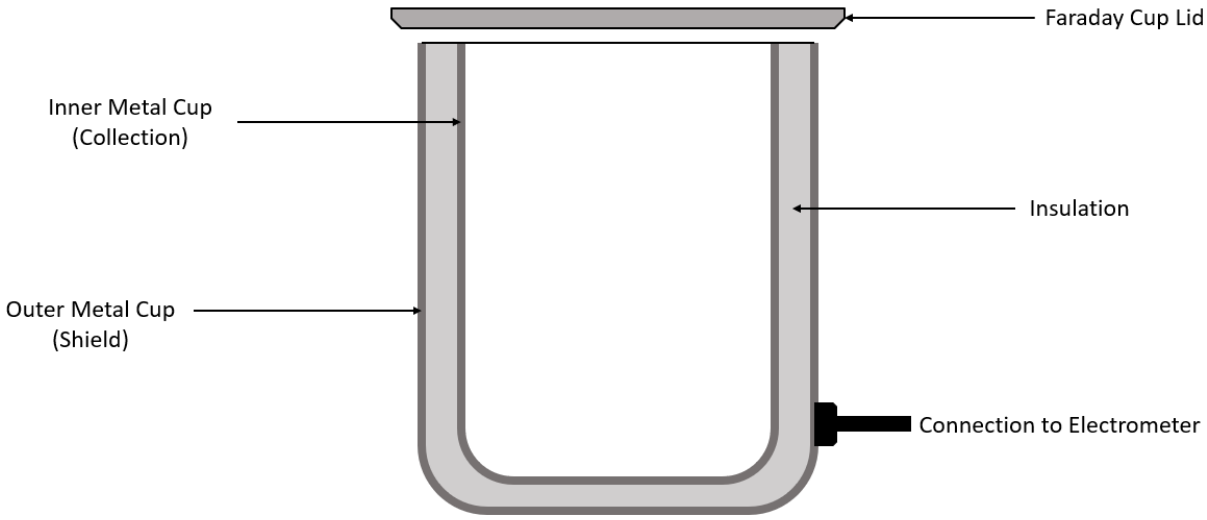

Figure 2. Labeled Faraday cup diagram.

On-line or in-line measurement is a form of measuring the current drop from one end of a system to the other. The current can then be transformed into charge (in coulombs) by finding the integration of the electrical current over time, as expressed in equation 4. In the equation charge, current and time are represented by Q, I, and t respectively.

$$Q = \int I \, dt \tag{4}$$

The set-up for on-line measurement can be completed with two methods, seen in Figure 3. The first method involves having two metal attachments. One metal attachment is present when the particles are initially released into the system and the other is placed at the end of the line where the particles will cease movement. Each metal attachment can be connected to an oscilloscope and the voltage drop from the initial to the final reading can be recorded (Schwindt, 2017). Once the voltage drop is retrieved, using the resistance of the circuit that has been created – the current can be calculated using equation 5.

$$I = \frac{V_d}{R} \tag{5}$$

Using the current calculated in equation 5, the charge of the particles that pass through the transporting line at that exact moment can be measured.

The second method for on-line measurement set-up requires connection to an electrometer rather than an oscilloscope and can measure current directly rather than use the conversion of voltage. This method demands a metal tube with an insulator at one end, the insulated end is connected to another part of the metal right at the stage of initial powder delivery. The

connections to the electrometer are made with the two metal attachments mentioned above and will only work with the insulator in between both metal pieces (Taghavivand, 2021).

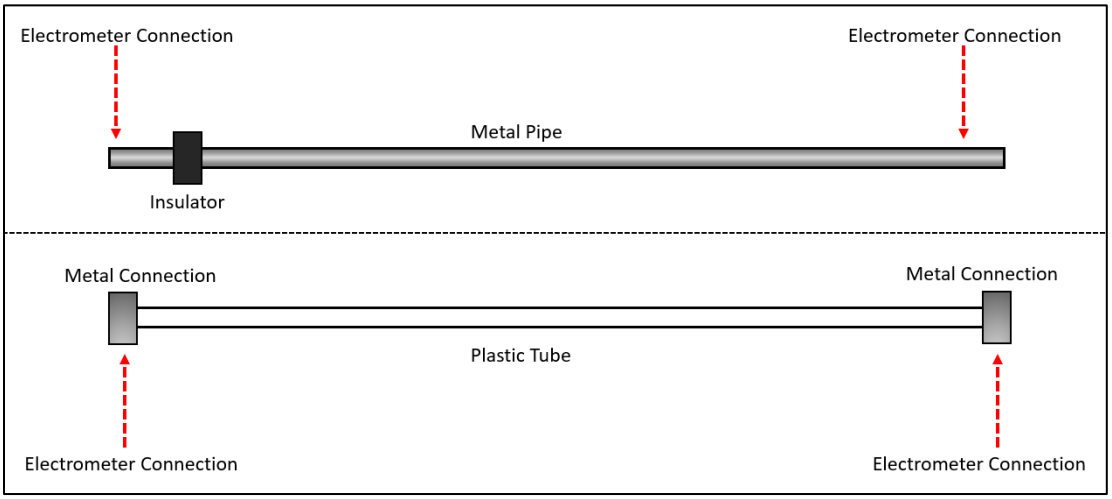

Figure 3. Methods for using on-line charging.

It is important to note that, unlike the Faraday cup, this method does not measure the total charge of all particles that move through the system, but as stated above, measures only the single moving particles that run through the system at the exact time.

Electric Low-Pressure Impactor (ELPI) is an instrument used to find real-time particle size distribution and concentration measurements within varying particle size ranges (Marjamäki et. al, 2000). The ELPI can be used for particle charge measurement and has the additional benefit of utilizing software to upload data onto a computer or hard drive for easy accessibility. As seen in Figure 4, the machine is comprised of a corona charger, vacuum pump, filter, and electrometers. The machine is capable of being connected to a computer and using its specific software can transfer data from the machine, such as particle size, sample distribution, and charge measurement. The process of measuring charge has the same principles of on-line charging, where current is measured at the beginning and end of

the pneumatic line, except within an ELPI there are multiple levels of electrometers (more than one) that are continuously monitoring the charge of the particles as they pass through the impactor (Telko et. al, 2007 & Chen et. al, 2015). Most research papers don't mention this machine, only a few predominately within the pharmaceutical research industry. This could be due to many factors, but the most probable reason would be accessibility and cost.

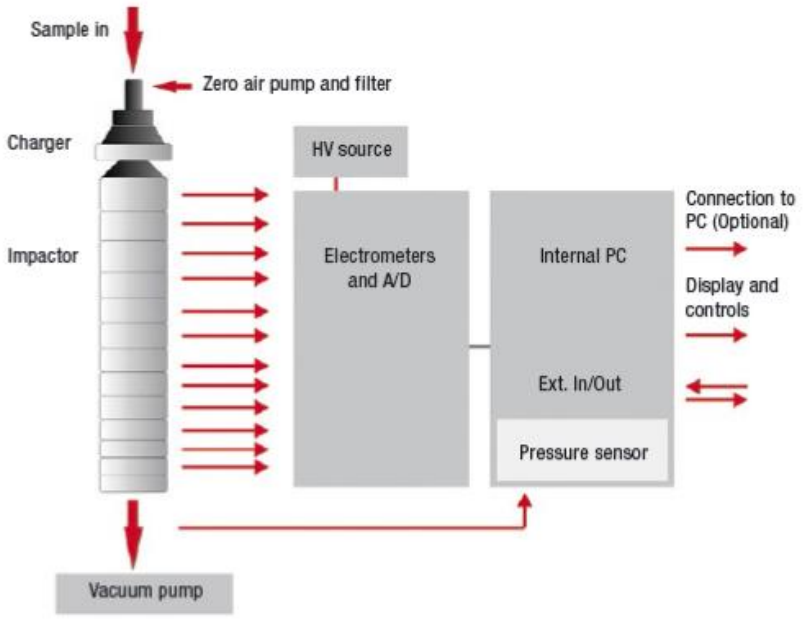

Figure 4. Diagram of ELPI Machine (Järvinen, 2014)

Electronic Single Particle Relaxation Time (ESPART) analyzer is an instrument used in electrostatic spraying to determine the size and charge of the particles, seen in Figure 5. This system is comprised of two parts, the laser doppler velocimeter (LDV) and the particle relaxation apparatus. The particles are transported through the system, passing through two lasers created by the LDV. The lasers and particle velocity are read by a receiving lens and a sinusoidal wave is formed. The amplitude and lag of the sinusoidal wave compared to its initial/base wave provide the charge and size distribution of the particles (Trigwell et. al,

2003). This appears to be similar to the ELPI, where the measurement apparatus is used in fewer research papers than both on-line measurements and the Faraday cup. This could be due to the specific equipment needed for the set-up. In addition, this seems to be equally as effective as all previously mentioned measurement systems. Therefore, seeing as this one requires the most detailed planning and organization of working components – it would be one of the least selected methods.

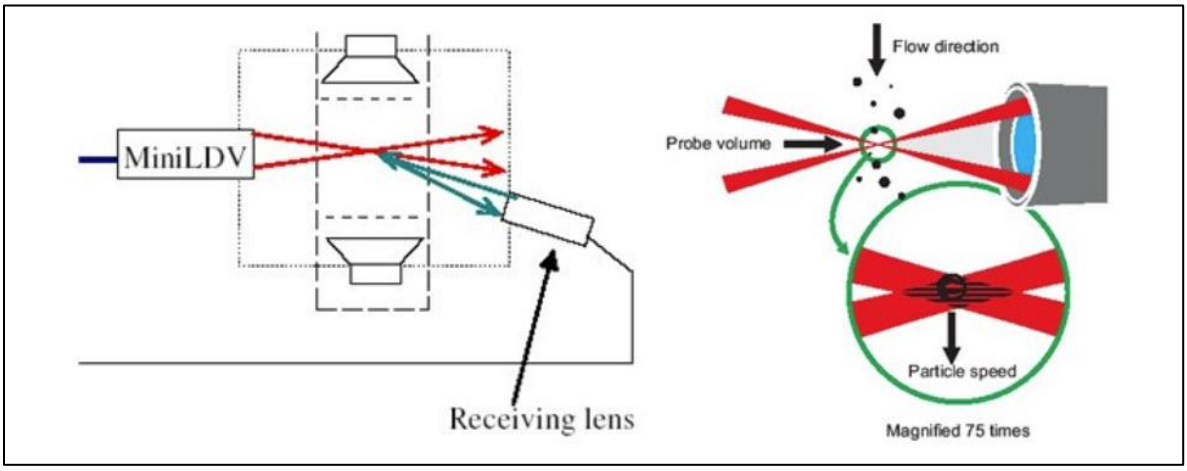

Figure 5. Diagram for ESPART charging system (Pierson, 2015).

Table 1. Research Papers Using Different Charge Measurement Apparatus

Measurement Method	Research Objective	Results	Reference
Faraday Cup	Investigating the charging behavior of sample powders utilizing a Faraday cup.	1. All the glass beads were negatively charged when stainless steel metal was used as the contact surface. 2. The charge-to-mass ratio of both powders increased as the applied air increased. 3. The charge of mass of the glass beads increased as the powder size decreased. 4. The charge amount of the glass beads increased with the length of the pipeline.	(Choi, Choi, and Suzuki, 2020)
	Investigating the effect of adding fines on the tribo-charging of glass beads.	1. The addition of small quantities of fines (up to 10 wt%) sharply increased the mass and surface charge densities of the mixtures. 2. When the particle–wall contact potential was greater for the coarse beads than for the fine particles, the absolute maximum magnitude of the mass charge density was achieved for the mixtures.	(Wang et. Al, 2018)
	Investigate which factors influence the charging process	1. From greatest to least effect on charge during aerosolization: flowrate of particles, addition of mannitol fines, and particle size.	(Karner and Urbanetz, 2013)

	during powder aerosolization and release from the inhaler.	2. When charging adhesive mixtures, additive pharmaceutical ingredients (API) cause a decrease, while the other factors cause increase in net charge	
	Observe the difference in tribo-charging DPI powders of varying surface roughness.	Rough powder exhibits significantly higher tribo-charge than smooth powder due to specific surface area and different rolling/transporting behavior can result in different charging behavior.	(Karner, Maier, Littringer and Urbanetz, 2014)
	Characterizing the triboelectric charging tendency of fine powders by impact using the smallest possible sample quantity with a pressure pulse.	1. The charge-to-mass ratio is larger for smaller glass sizes, due to the increase in total surface area of the sample in a given volume. 2. Due to "space charge effect" (limitation of current flow due to electrons repulsion from both charging materials) a decrease in charge-to-mass ratio for sample volumes of 7 and 9 mm^3, while smaller sample volumes remain constant. 3. Functional groups exposed on the surface of the particles greatly influenced the tribo-charging. -CF3 functional group charged negatively, while -CH3 and -NH2 charged positively. 4. Charge is dependent on the work function of the surface material.	(Zafar, Alfano and Ghadiri, 2018)

	Compare surrounding factors for charging of polymers including humidity, surface composition, acid-base properties (acceptor/donor properties), surface resistivity, and water absorption.	1. Polymers with high electron pair donor strength show a higher basicity and should have a high electron pair accepter donor (high acidity). 2. The predominate character of an electron pair (donator or acceptor) determined the sign of the total surface charge. 3. Water can support the discharging of polymer surfaces. Water molecules can be adsorbed from the wet atmosphere or can be contained in the polymer.	(Nemeth, Albrecht, Schubert, and Simon, 2003)
On-line Measurement	Investigation of on-line measurement and external factors that affect the charge measurement. The latter half, investigates wall fouling that occurs at the end of the pipe.	1. For large particles moving in straight tubes, the lowest gas velocity resulted in higher charge-to-mass ratio. The particles pathway had a large impact on charging behavior at high gas velocities, whereas at the lowest gas velocity, the total tube length was more significant on particles charging. 2. Results showed a relationship between the conveying line length and the powders' charging. Changing the pathway did not show a significant effect. 3. Results showed a relationship between the bulk of the bed net charge magnitude and wall fouling. The bed bulk charge and the wall fouling magnitude was varied by the type and concentration of the additives.	(Taghavivand, 2021)

	Experimental study of the influence of a range of parameters within the tribo-charging of powders and transport pipes.	1. The powder charge first increases with increasing conveying air velocity until it reaches a maximum (saturation point) beyond which it drops. 2. The air velocity that maximizes the powder charge depends on the pipe material, diameter, and powder mass loadings. 3. Tests showed that the powder charge increases significantly with the inner diameter of the transport pipe.	(Schwindt et. al, 2017)
Electric Low-Pressure Impactor (ELPI)	Observe the influence of tribo-charging on dry powder inhalers (DPI) and analyze external factors.	1. Main contributor to the overall charge was the tribo-charging was during the DPIs actuation and the charge captured with ELPI to be within a range of 100-1000fc. 2. The morphology of the lactose powder primarily promotes the tribo-charging, and different morphology could change polarity.	(Telko, Kujanpää and Hickey, 2006)
	Investigate wall to particle contact using various (looking for another word for design or curvature) and materials.	1. The design of the contact surface has no effect on charge distribution for the aerosol but significantly influences charge polarity. 2. Curved nozzles (for PET and PTFE) significantly impacted charge polarity due to plume geometry caused by the curve edge and bipolar charging of insulating materials.	(Chen et al., 2015)

Electronic Single Particle Relaxation Time (ESPART)	Effects of Surface Properties on the Tribo-charging Characteristics of Polymer Powder as Applied to Industrial Processes	1. Bipolar charging was observed for each powder. The highest level of unipolar charging against stainless steel (net negative) was observed for the polyester powder. 2. A linear relationship between the mean charge vs. particle area was observed. In both powders, it was observed that the polarity was negative compared to the positive charge from the larger size particles. 3. Work function differences between the powder and charging material and powder particle size were significant factors.	(Trigwell et. al, 2003)

2.4. Factors Affecting Charge

As seen in table 1, research has concluded that different factors can affect the tribo-charging of particles. The main contributing factors are work function, size, shape, surface morphology, and humidity.

The work function, as previously stated above, is the minimum quantity of energy which is required to remove an electron from the surface of a given solid (Trigwell et. al, 2003). This can affect the charging of the particles, as the work function of different powders show the charging capabilities as the electrons jump from one material to the next. In tribo-charging, this electron transfer would be between particles-to-wall or particles-to-particle contact. In addition to the traditional or simpler equation for contact potential difference, Matsusaka was able to derive a formula to solve for charge-mass ratio which can be rearranged for the contact potential difference (Matsusaka, Shuji, et al, 2010).

$$V_c = \frac{\pi \Delta q D_p^3 \rho_p z_0}{6\varepsilon_0 n(x) k S m_p} \tag{6}$$

Equation 6 has contact potential equal the product of total charge (Δq), pi, the diameter of the particle cubed (D_p^3), the density of the particles (ρ_p), and critical gap between the particle and wall (z_0); divided by the product of dielectric permittivity (ε_0), number of particle collisions ($n(x)$), charging efficiency (k), contact difference (S), and mass of the particles (m_p). The contact difference can be calculated using equation 7, where v_i is the impact velocity of the particle which can be calculated using equation 8 and k_e is the elasticity parameter, which can be calculated using equation 9.

$$S = 1.36 k_e^{2/5} \rho_p^{2/5} D_p^2 v_i^{4/5} \quad (7)$$

$$v_i = \frac{\mu Re}{\rho_0 d} \quad (8)$$

$$k_e = \frac{1 - v_1^2}{E_1} + \frac{1 - v_2^2}{E_2} \quad (9)$$

In equation 8 calculating impact velocity, μ is the viscosity coefficient, Re is the Reynolds numbers, d is the diameter of the tube, and ρ_o is the density of air. Equation 9 calculated the elasticity parameter, using $v_{1\text{-}2}$, as the poison ratio and $E_{1\text{-}2}$ as the Young's Modulus for both particle and wall (Mehrtash, 2021).

The size of the particles often contributes to charge as well. The smaller the size of the particle, the greater possibility of a larger portion of the particle coming into contact with the contact surface. The larger surface area creating contact with the wall causes a higher charge, therefore creating a higher charge-mass ratio. Mikrowska et al. published a literature review on the methodology and factors affecting triboelectrostatic separation specifically for minerals. Within her report, an equation for charge density was used (equation 10), where ε0 is the permittivity of the carrier gas, ε is the permittivity of the insulator, V_c is the contact potential difference and x is the thickness of the insulator (Mikrowska et. al, 2016).

$$\rho_s = 2\varepsilon_0 \varepsilon \left(\frac{V_C}{x}\right) \quad (10)$$

Knowing that charge density is equal to the charge of the particle divided by the volume of the particle. With the assumption of uniform and spherical particles, equation 10 can be rewritten where d_p is the diameter of the particle, and Δq is the charge of the particle.

$$\left(\frac{d_p}{2}\right)^3 = \frac{3\Delta q}{8\pi\varepsilon_0\varepsilon\left(\frac{V_C}{x}\right)} \quad (11)$$

Research completed by Laundauer, and his team, displayed that the charge collected by experiments comes from particle-to-wall collisions, rather than particle-to-particle. This is due to the size of the particles being small, while the surface material is usually quite large. The small particles hitting each other is less likely than the particles hitting the larger wall – causing more collisions. The more collisions, the more charge is transferred – showing that the wall-particle collisions make up a majority of the collisions and the charge (Landauer, Johann, et al, 2019). Research with a contrasting view however comes from Cruise. They depict that the smaller the particles, the more can fit through tubes and collide with each other and the wall. This can create an increase in charge through particle-to-particle collisions (Cruise et. al, 2022).

The morphology of the powders is another charge-affecting factor and can include spherical nature, and roughness. Research completed by Karner et. al, indicated that when particles are closer to a spherical shape the tribo-charge will increase. This is due to more spherical particles having a more uniform charge distribution while shriveled or non-spherical particles may not have proper contact with the walls to create collisions/charge. In addition, the non-spherical particles may have less residence time within the inhaler, therefore less of a chance to charge within the walls – this is due to the direct correlation between aerodynamic diameter and residence time (Karner, Stefan et. al, 2014). Another example of research completed showing the effect of surface morphology within tribo-charging is from Wang et. al. The study was conducted using both rough and fine glass beads in addition to

fine particles with rough and fine coatings of stainless steel. The results indicated that when fine coatings were added to the already coarse particles, little change occurred – however after the coating was equal to approximately 10% of the weight of the particles the mass and surface charge densities of the mixtures were both increased. In addition, the fines with the 10% weight increase caused higher charge generation and that the tribo-charging of the mixture of particles was dominated by the coarse particles contact with the wall or material of pipe (Wang, Haifeng, et al, 2019). Research completed by Mehrani et al, experiments were performed to determine the factor affecting electrostatic charges of particles within a fluidized bed using different fines or particles of varying surface roughness and material. The research results show that the work function of the particles can be affected by the roughness of the particles, as not smooth particles with crack leave areas where the particle will get less saturation (Mehrani et al, 2007). However, Mehrani's results for particle size differ from the findings of Zhang et al. Mehrani reports that larger particles should collect electron transfer from the smaller particles – while Zhang reported that when small particles contact larger particles, electrons should transfer from larger particles to smaller particles. This results in smaller particles becoming negatively charged, while the larger particles become positively charged. The difference in findings could be due to surface impurities of particles that affect their work function at the point of contact (Zhang, Guangwen, et al, 2013).

Humidity is the measure of the amount of water vapor absorbed into particles (Aríñez-Soriano et. al, 2016). This can affect tribo-charging, as the moisture absorption within a particle increases, the composition of the particle may change, causing the typical charging of the particle to adapt and adjust the rate of charge. (Xiaosong Ma, et al, 2007 & Marchetti,

Lorenzo, et al, 2022). Surface conductivity plays a key role in triboelectrification and is strongly influenced by water adsorption (Yanar & Kwetkus, 1995). A study written by Yanar and Kwetkus looked at how humidity affected the separation of two polymers (PE and PVC). The study showed the separation of PE and PVC was greatly decreased with the increase of humidity, meaning that the charges collected by PE and PVC to perform separation had decreased significantly (Yanar & Kwetkus, 1995). Another paper written by Albrecht, Janke, Nemeth, and others, investigated charge density vs. many external factors including humidity. The results indicated that even though the results of water absorption are different per polymer, all show the results of discharging of the polymer surfaces when water absorption is increased. This is due to water molecules being able to dissociate by themselves and form hydrogen ions and hydroxyl ions which act as charge carriers – removing the charge from the polymer particles (Albrecht, Victoria, et al, 2009). Research completed by Kolehmainen et al. studied the effect of humidity on triboelectric charging using vibration as the methodology for transporting the particles. Both physical experiments and mathematical modeling were completed to obtain data and validate results. Looking at an equation presented in the report – the relative humidity of the system could be written using the following equation. Where $\frac{Q}{m\Sigma}$ is the charge-mass ratio and ϕH is the relative humidity. Modelling parameters such as ρ_s, ϕH_0, and ΦH were obtained using linear least square regression using the data collected from the physical testing.

$$\frac{Q}{\mathrm{m}\Sigma} = \rho_q \left(1 - exp\left[-\Phi \mathrm{H} \left(1 - \frac{\phi H}{\phi H_0}\right)^2\right]\right) \tag{12}$$

The results of the research depicted that the work function of the charged particles is dependent on the relative humidity. Using an equation similar to equation 12, the

dependency of the work function ($\varphi_{(\phi H)}$) can be determined, where φ is the effective work function (Kolehmainen et. al, 2017).

$$\varphi_{\phi H} = \frac{\rho_q \left(1 - exp\left[-\Phi H \left(1 - \frac{\phi H}{\phi H_0}\right)^2\right]\right)}{1 - \exp[-\Phi H]} \varphi \tag{13}$$

Supporting the research previously cited is from Nemeth, Simon, and others - an increase in the atmospheric humidity strongly influences the charging behavior of polymers. The reason for the humidity influence on the charging and discharging behavior of polymers can be explained by the formation of water films onto polymer surfaces. Some of the polymers (PA, PMMA, and POM) have a high ability to take up water (Németh, Ernő, et al, 2003).

Chapter 3. Methodology

Creating a particle delivery system was determined to be the first step in assembling the system, as the movement of particles is necessary to produce tribo-charging within a pipe or tube with airflow. The objective of this section of the system was to have a consistent flow of particles being transported to the measuring portion of the machine. While consistent delivery is not necessary to collect charge of the particles, it would be beneficial for collecting and measuring the charge-to-mass ratio. The next section of the tribo-charging system to be designed and manufactured should be the charge measurement. When designing the charge measurement system, the objective is to have it reliably provide data on the obtained charge of the particles that pass through the system. There have been 3 different designs created for the mass delivery, and 2 for the charge measurement – they will be outlined in the following sections.

3.1. Methodology for Particle Delivery Design

When deciding upon the correct device for particle delivery, three methods were available: vibration, fluidized bed, or screw feeder. The vibration method uses a vibrator to move the particles along either a slide or a tube. This method has the capability of making the powder cluster together and there is no way to ensure that the powder will continue moving. This could result in inconsistent flow. (Limtrakul, Sunun, et al, 2007).

A fluidized bed is created using an air-sealed container with the powder which pressurized air is passed through. The pressurized air caused the particles to become airborne and allow

them to be transported through a tube to their desired location (Ali, Syed Sadiq, et al, 2021). While this method can produce a steady flow of particles, the fluidized bed has many external and internal factors that can cause malfunctions and result in inconsistent particle delivery. Examples are the mass of particles inside the bed, air resistance of the airflow within the fluidized bed, and the location of the particles within the bed with respect to the airflow entrance/exit. Therefore, there are many concerns about achieving consistent mass of particle delivery with this method.

Finally, screw feeders are a method with an auger being used to mill through the powder as it goes from a hopper or containment device into its new location (Fayed, 1997). This method can solve the issue of having inconsistent mass delivery and "clumping" of powder within the system. However, screw feeders are both expensive, and smaller research models are harder to come by. In addition, making a screw feeder can be quite complex, and specific equipment needs to be manufactured rather than purchased.

3.1.1. Particle Delivery Design #1

To design the first particle delivery set-up, the different particle delivery methods were researched and compared to find a reasonable fit for the project objectives. Seeing as consistent mass delivery was determined to be important, the screw feeder was chosen as the first design for particle delivery. The parts were designed using Autofusion 360 and printed using the Prusa 3D printer. To guarantee the particles would not cluster together from the hopper to the screw feeder, the screw feeder was mounted on top of a vibrator and used in tandem.

The measurement system set-up, seen in Figure 6, is comprised of an air drier, hygrometer, flowmeter, powder delivery device, faraday cup, electrometer, and weight or balance. The air drier, hygrometer, and flowmeter are used to provide consistent airflow, adding temperature and humidity control into the system. The powder delivery is comprised of a vibrator, screw feeder, and a hopper. The airflow used in the system is connected to the top of the hopper and the exiting-end of the screw feeder. The screw feeder is then connected to a motor, once turned on the auger rotates with the cylindrical part of the screw feeder providing a consistent delivery from the initial connection at the hopper to the exit at the bottom.

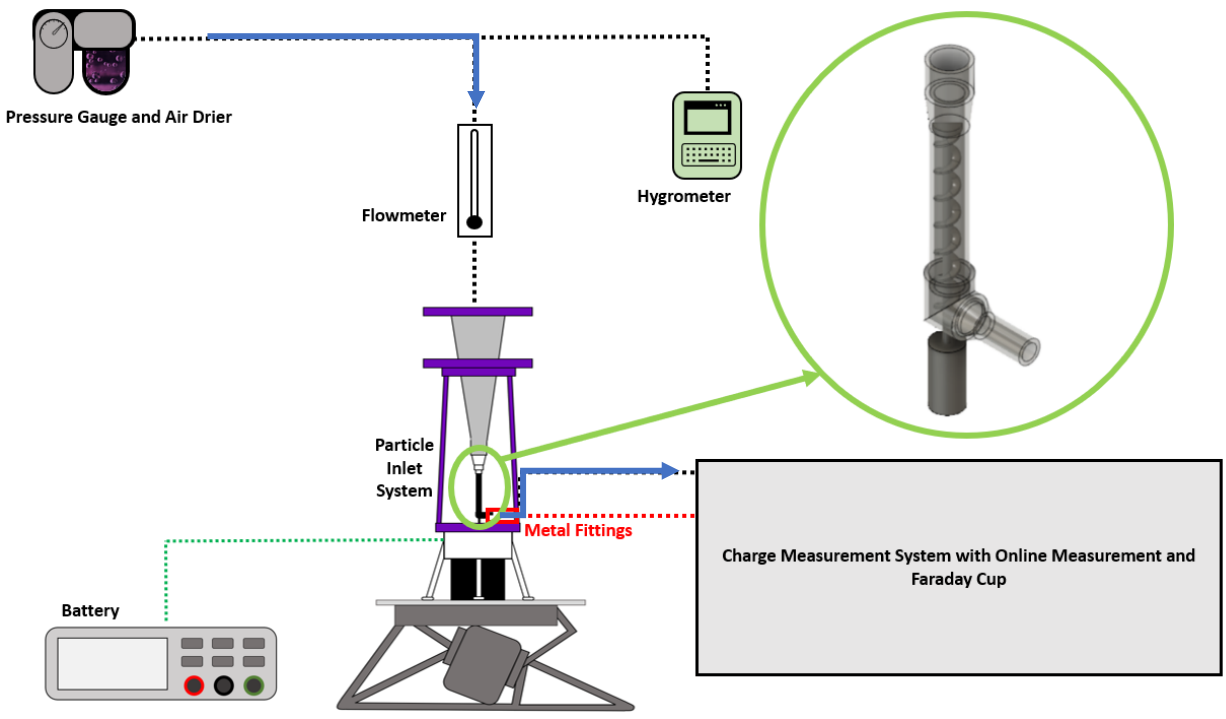

Figure 6. Schematic for Delivery System with screw feeder and vibrator combination.

3.1.2. Particle Delivery Design #2

The second delivery method was a fluidized bed. When this method is used properly, it can give a steady stream of particles. Fluidized beds have the tendency of having the powder stay stagnant within the container. When the powder stays stagnant, only the powder directly in front of the airflow entrance will move and flow out of the exit tube. Once again to stop the powder from staying stagnant inside the container, the fluidized bed was mounted on top of a vibrator and used in tandem. The second design can be seen in Figure 7, and the blue arrows on the picture show the flow of air. The airflow goes in through the bottom of the container, powder and pressurized air come out through the top using a 3/16" OD and 1/8" ID tube. The tube then leads to the Faraday cup being placed on a mass balance. The tube is held using clamps and a pole, so the effects of vibration will not affect the balance. A specific lid had to be created for the Faraday cup to prevent powder from leaking out of the cup and skewing the mass collected by the balance. The lid was created using Autofusion and printed using a Prusa3D printer. 3D and 2D drawings of the lid can be seen in the appendix, section7.

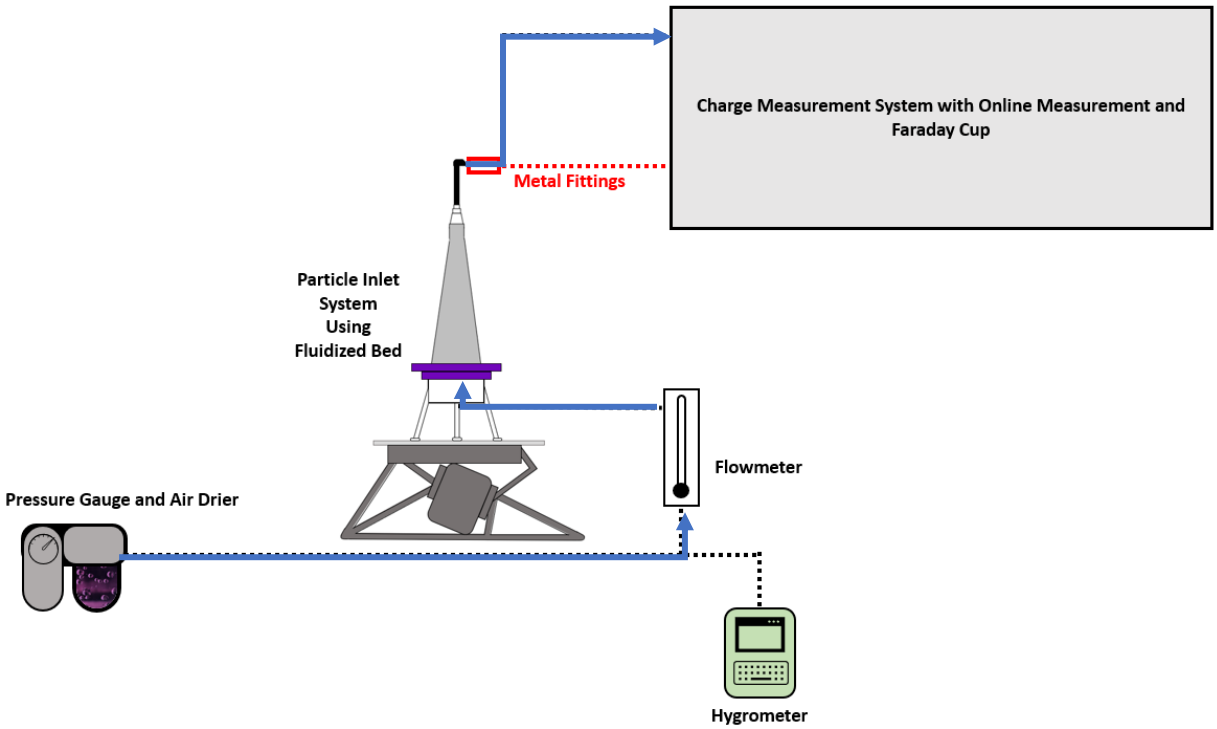

Figure 7. Schematic of 2nd particle delivery design utilizing a fluidized bed and vibrator combination.

3.1.3. Particle Delivery Design #3

The third, and current, mass delivery design removes the objective for a consistent mass delivery rate – but only a constant mass being produced. This mass delivery system would be implemented for an offline system, rather than online – meaning the mass would be read/collected before and after the trial is run rather than during.

Figure 8, shows the new mass delivery system. The design still uses a fluidized bed, but with a new orientation. The new orientation is to remove any possible issues with delivery caused by the location of powder within the hopper. In addition, the input/output of airflow has been swapped. The new mass delivery system works as such: take the initial mass of the Faraday cup, turn on air and allow particles to enter the system for a certain period of time,

take final mass of the Faraday cup, and calculate difference in mass to achieve the net mass. In addition, the lid for the hopper has been redesigned for easy access to the powder within the hopper. This is done to make the time between trials faster.

Figure 8. Current mass delivery design. New orientation of the fluidized bed and a new way to access the inside of the hopper to make adding powder quicker and accessible.

Adjustments to the Faraday cup lid were also made to help with the tightening of the lid to the Faraday cup. The design was completed in Autofusion 360 and printed using PrusaSlicer.

Therefore, tests will be run to determine if mass delivery can be constant and if the new orientation of the fluidized bed with an increase in airflow can result in consistent delivery. The charge measurement should be able to measure the charge at the same time as the mass delivery. Each section of the charge/mass will have to be compared to see if for each time

step the difference in both mass and charge is consistent. In the next section, the charge measurement system will be designed and constructed.

3.2. Methodology of Charge Measurement

Seeing as both online and offline charge measurement systems would be needed to accommodate the mass delivery designs #1-3, two separate designs were created and manufactured. Online measurement means that real-time data for the charge and mass are being collected to obtain the charge-mass ratio at that exact time frame. While offline measurement means that the initial and final values for both charge and mass are collected, and the net values for both are used to obtain the charge-mass ratio. The first design was an online charge measurement system with a Faraday cup as a verification system, and the second design was an offline charge measurement system using solely a Faraday cup connected to an electrometer.

3.2.1 Charge Measurement Design #1

The two methods chosen for this system are an on-line measurement system and a Faraday cup. The Faraday cup is used for verification, while the on-line system would be used for the initial measurement. This was decided due to the simplicity of design for the on-line measurement with easy and reliable charge results. The Faraday cup would be good for validation, as many research articles use this method and they all show acceptable results. The reason the Faraday cup isn't the main charge measurement device is because the Faraday cup measures the total amount of powder's charge, while on-line measures individual particles' charge. This means additional steps would need to be taken to calculate the charge of the particles using the Faraday cup.

To compare the Faraday cup results with the on-line systems charges, the mass vs. time collected by the balance must be matched up to the charge vs. time. Then the individual seconds are compared for mass and charge to get a mass-charge ratio for each second the system is in use. These results are then compared to the on-line system's data collected per second using an oscilloscope.

Figure 9 displays the on-line measurement system with connections with respect to the Faraday cup. The metal attachments are rigged up to an oscilloscope with an amplifier in the middle. The amplifier is used to magnify the charge to read the charge on the graphs. The magnification is x10^7. The oscilloscope measures voltage drop between the initial starting of the powder leaving the fluidized bed and the whole tube covered in aluminum. The tube is covered in aluminum and acts the same as using a completely metal tube. As the charges from the particles pass through the plastic tubing, it goes to the aluminum foil and the charge on the foil gets read by the oscilloscope. Figure 10 displays the schematic for the voltage to charge conversion. Using the oscilloscope and the amplifying circuit, the voltage is measured. Already knowing the capacitance of the circuit, the following equation can be used to calculate the charge of the particles within the system, where V_{out} is the voltage drop, C is the capacitance, and Q_{in} is the charged particles (Galayko et. al, 2015)

$$V_{out} = \frac{Q_{in}}{C} \tag{14}$$

The Faraday cup is at the end of the system and will be attached to an electrometer. The electrometer will be used to measure the charge over a period of time. As stated above, it will be the charge of the total amount of powder collected inside the cup. The charge will have to

be divided by the mass of the powder collected by the balance, to obtain the mass-charge ratio of the powder.

If the particle delivery from the previous designs is not consistent, charge cannot be looked over a large section of time, it must be looked at each time interval individually to see if the charge is consistently being measured throughout the whole testing time interval.

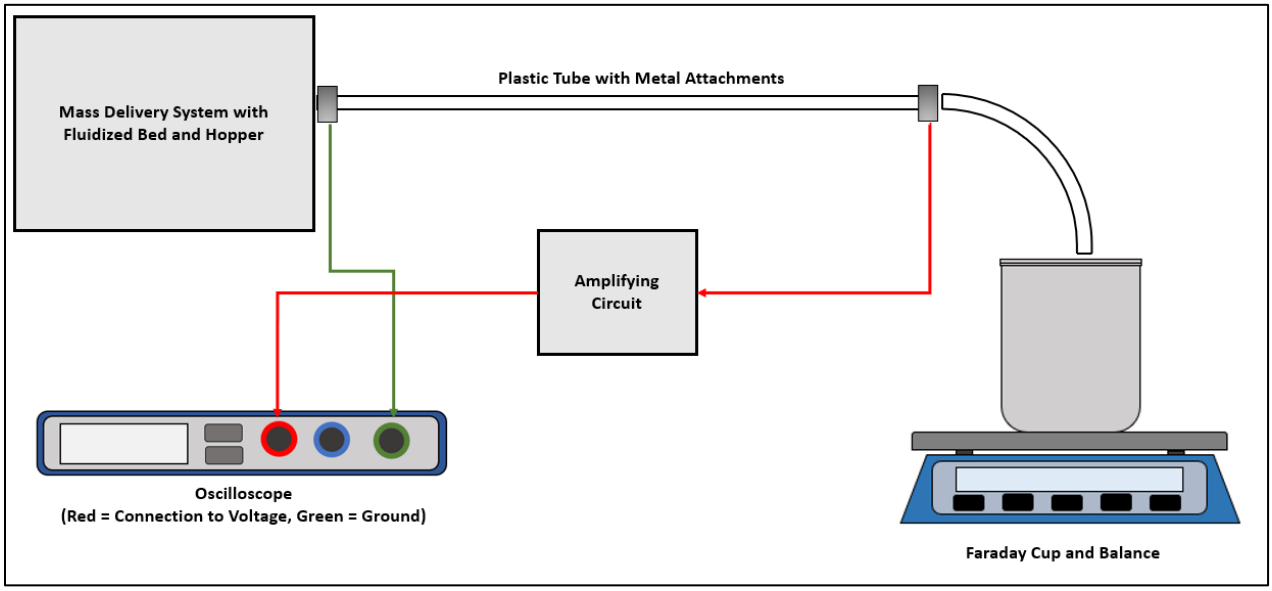

Figure 9. Diagram of on-line measurement system initial design.

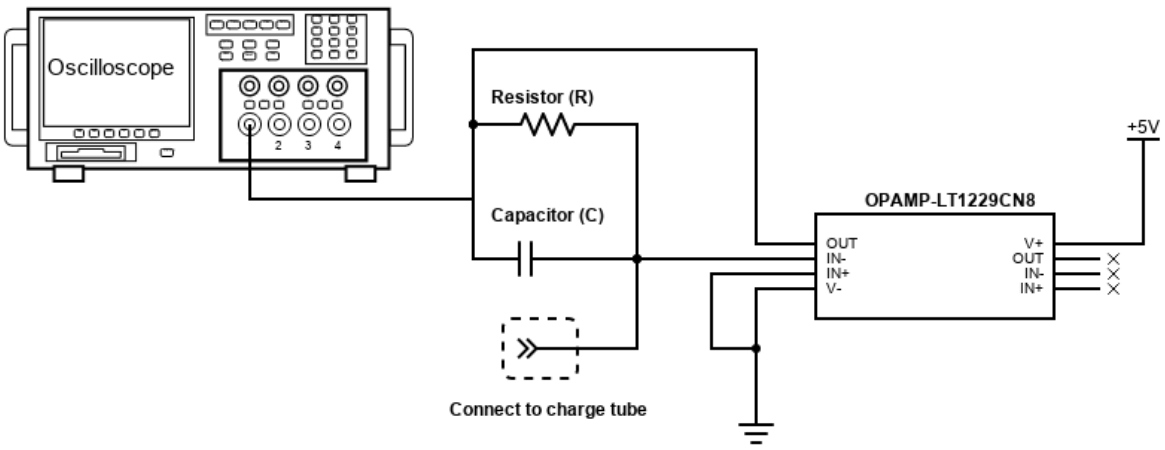

Figure 10. Schematic for charge to voltage converter.

3.2.2. Charge Measurement Design #2

The second design for the charge measurement was designed and constructed. This design was intended to be implemented with particle delivery design #3, as both designs were created to not have data collected in real-time. A 3D-CAD model of the new design was created in Autofusion and can be seen in Figure 11. The new design depicts copper tubing being formed into a helical shape inside a plexi-glass cylinder. This should assist in making sure loose powder does not affect other electrical equipment, as it will be contained. In addition, to ensure that the charged powder will not cause any extra problems, the charging measurement section of the system will be in its separate location – away from the electrical devices. The charge measurement coil is grounded, as the tests being completed are offline. Therefore, the connection to the electrometer will now be stationed at the end of the Faraday cup – rather than attached to the metal coil.

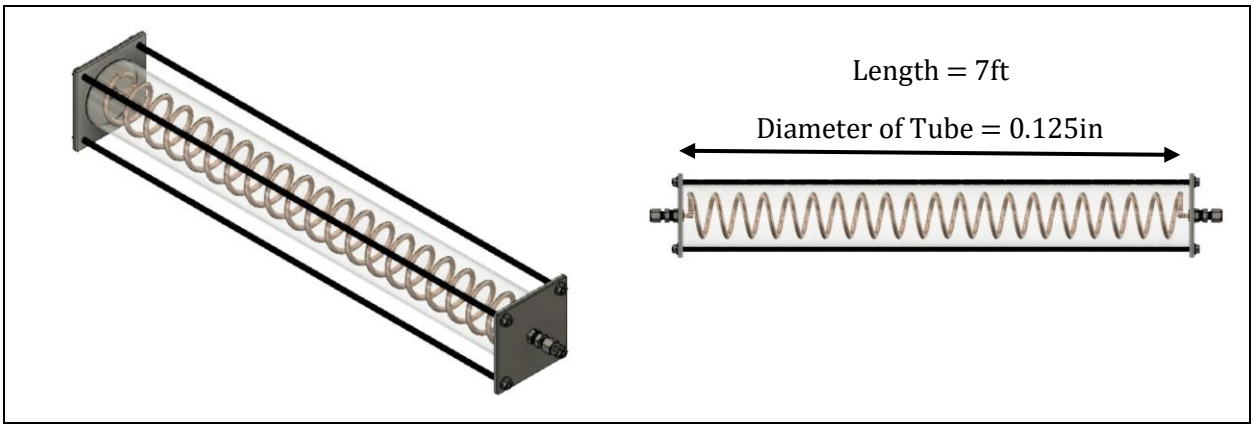

Figure 11. Second Design for Charge Measurement

Figure 12 depicts the new charge setup. To ensure that the charged powder does not affect any of the electrical equipment, a cylinder has been constructed to surround the Faraday cup and the cup has been coated in conductive paint to ground the section of the system. As of now, the charge will start at "0" initially, and after a period of time with the system running the final charge will be collected. A net charge for the system will be completed (taking the initial charge and subtracting the final charge).

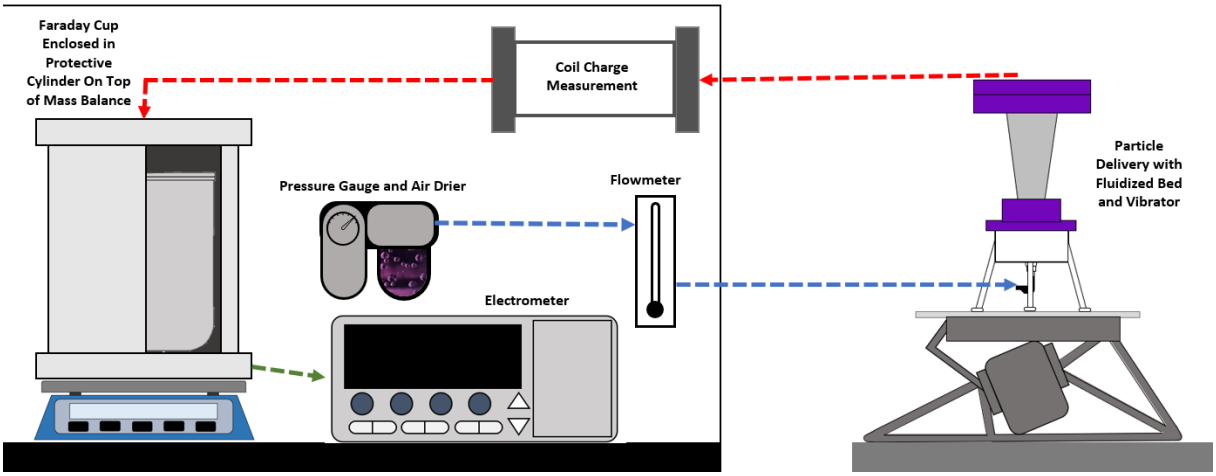

Figure 12. Schematic of new charge measurement and mass delivery system. The blue arrows indicate airflow, the red arrows indicate airflow with particles, and the green arrow

indicates the charge measurement aspect of the offline system once the mass has been measured.

3.3. Methodology of Size Distribution and Protein Content Testing

Both size distribution and protein content tests are necessary to make sense of the data collected from the real time tests. Size distribution tests are necessary as each powder has varying particle size ranges, density, and other physical characteristics that can affect the flowability of the powders and the particles' ability to be charged. Protein content testing was determined necessary for experiments using different powders mixed together and experiments where the same powder has been sifted into size ranges. For experiments where pure powder mixture were used, protein content was determined necessary as the ratio collect at the end of the system could not be confirmed as the same ratio that started at the entrance of the system. Experiments using different size ranges of the same pure powder used the protein content testing to determine if the sifted size ranges have different protein contents and if that has an effect on the charge.

3.3.1. Particle Size Distribution Test

Particle size distribution tests were completed using the software, ImageJ. ImageJ is an image rendering software that provides the tools to isolate the particles and determine the area of the particles shown in the pictures. The data can be organized and using the mean surface average equation, the standard deviation and mean diameter of the particles can be calculated. Histograms or scatter plots can be used to obtain a visual aid of the total scale of size for each of the particles analyzed.

3.3.2. Protein Content Test

The protein content test was completed using the Bradford Assay. This method requires the powder to be prepared first by rehydrating the powder first with water and adjusting the pH of the solution using NaOH. To prepare the Bradford reagent necessary for the Bradford Assay, bovine serum albumin (BSA) is diluted with water and placed in a microcentrifuge tube within a spectrophotometer. Using a blank tube containing water and the Bradford reagent is mixed and absorbance readings are taken as a baseline. The assay is completed by adding the powder to the Bradford reagent in microcentrifuge tubes. The mixture is inverted, and absorbance readings are taken.

Chapter 4. Results and Discussion

4.1. Particle Delivery Plan #1

Initially, airflow, diameter of tubing attached to the screw feeder, and mass of powders were changed to determine the effects for particle delivery. It was seen that as airflow into the system increases, the time of delivery decreases. In addition, as mass increases – the time for delivery increases, and as the diameter of the particles increases, time for delivery decreases. Even with the slowest airflow, and smallest diameter of particles, the time for the particles to be delivered was extremely fast. This would not be acceptable, as the main objective is constant mass delivery over a long enough period that the on-line system will be able to collect measurements for both change in mass and charge over time. The reason for the extremely fast powder delivery could be due to the powder going down to the screw feeder in a downwards motion, the force of gravity forcing the powders downwards and the force of the airflow acting as a jet could have been making the powder exit the hopper at a high velocity – regardless of the other variable adjusted (Clayton, 2018).

Figure 13 shows the mass delivery of the screw feeder at 15 LPM for 10 grams. Looking at the graphs provided for the mass using the screw feeders, the fluctuations in masses can be seen. None of the trials over the same period of time have the same mass increase. The fluctuations are coming from the high velocity of the airflow as it rushes through the system (Marefatallah, 2019). To use the screw feeder, fluctuations would need to be accounted for and the mass would have to be calculated for each time step. With both the extremely fast delivery and the fluctuation of mass results, it was concluded that the screw feeder was not suitable for this project's objective and a new delivery plan would have to be implemented.

Another issue with the design was the contact created by the tube and the inside wall of the Faraday cup. The balance measures the force of the mass (force of mass = weight × gravity) on top of the scale. Since this contact was occurring, an extra force was being placed on the cup and was skewing the mass results. Even though the tube within the cup was at an equilibrium – the force being applied was not and with the addition of the vibrator shaking the tube inside the cup, the force was also constantly changing. In most cases, while measuring mass this could be negligible – however the amount of powder being measured is so small –any small changes caused by outside forces affect the balance. Therefore, in order to prevent this extra force, the tube cannot touch any part of the cup or fixture that comes in contact with the cup on top of the mass balance.

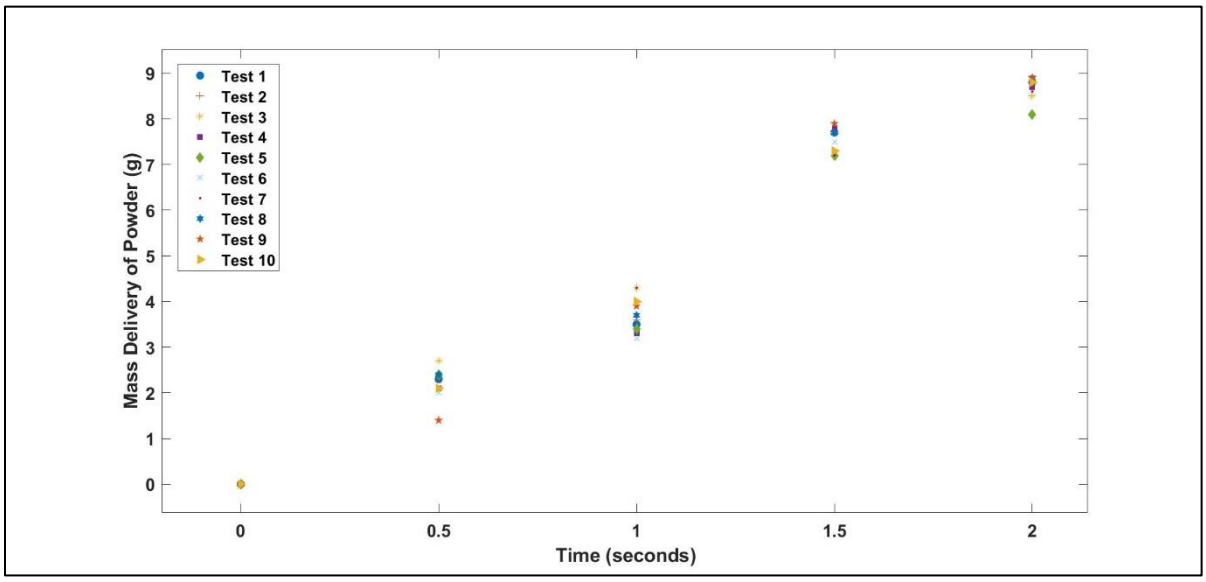

Figure 13. Graph of initial mass delivery vs. time results over 10 trial runs.

4.2. Particle Delivery Design #2

Results of the fluidized bed delivery system at 15 LPM using 10g +/- 1g of powder for 2.5 minutes are displayed below in Figure 14. The results show the same trend or shape of powder delivery; however, the mass delivery is not the same each time, proving there is some difference in the conditions that result in different amounts of mass being delivered each time. Any of the previously mentioned issues with fluidized beds could be the reason that the results are not repeatable. However, it is possible that with higher airflow, many of the issues can become negligible. It was concluded that continuous particle delivery is possible using the fluidized bed/vibrator hybrid, it just is not consistent delivery over a period. Although it was not a reproducible mass delivery, instead of measuring the absolute value of the charge, it was decided to report the charge per mass. The measurement of charge per mass could correct this variability of the mass delivery.

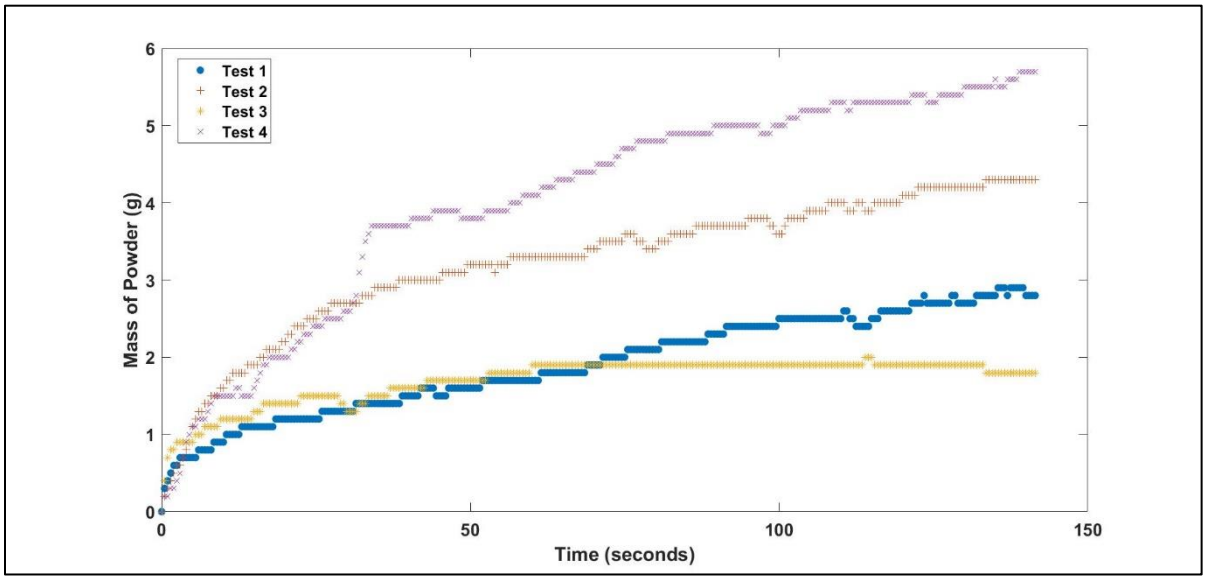

Figure 14. Graph for data collected from fluidized bed mass delivery vs. time.

4.3. Charge Measurement Design #1

Using the charge measurement system, the following graphs could be obtained, as shown in Figure 15

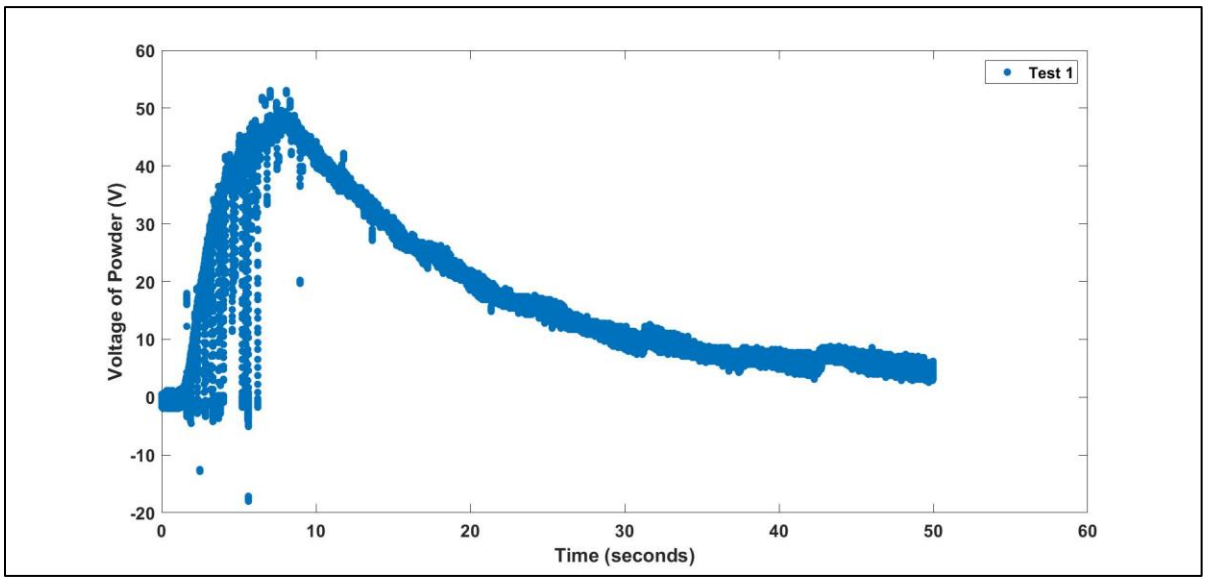

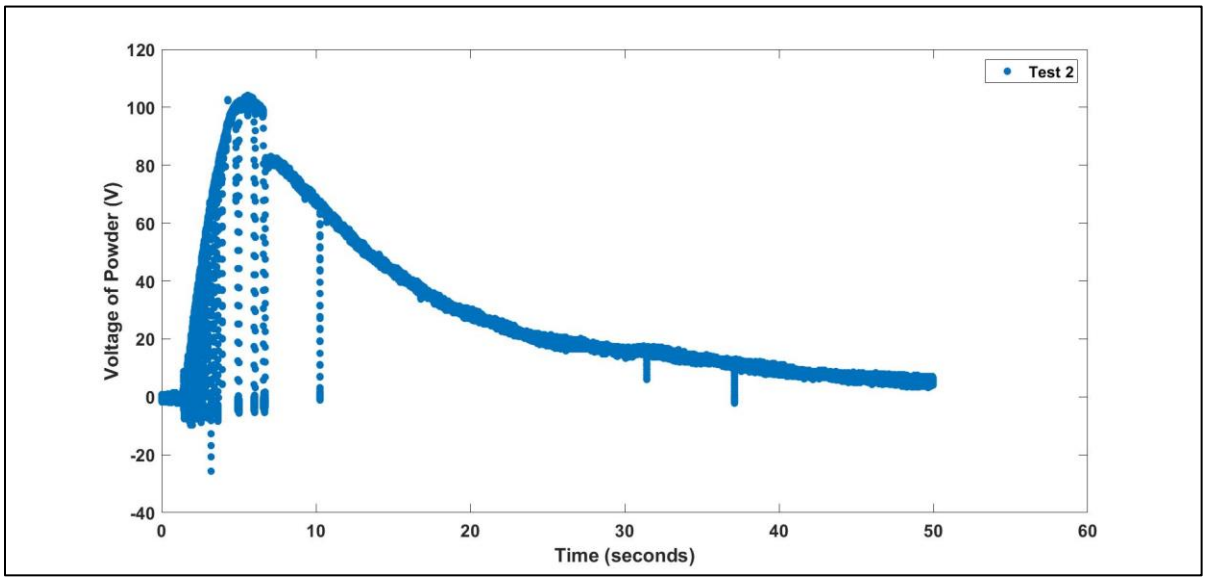

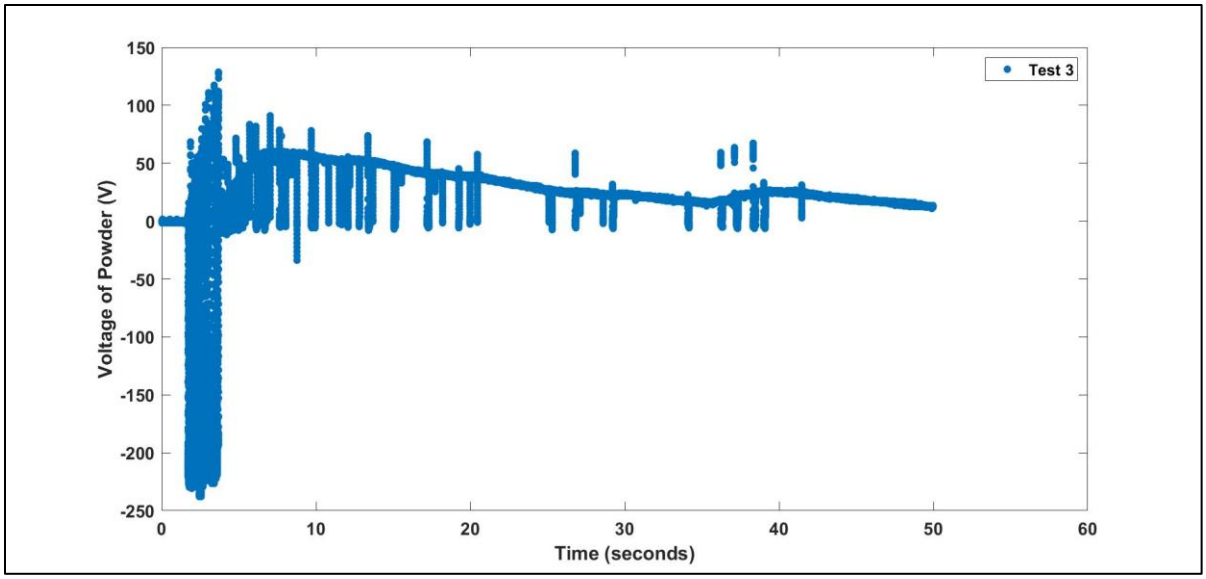

a-c. As seen in the graphs, there is an initial spike to a certain voltage and decrease until the voltage reaches 0v. This makes sense – to measure the voltage the ADC ground the circuit reducing it to zero. But charge is the integral of current (area under the voltage curve) which will not be zero. The data collected and graphed by Taghavivand shares the same trend when looking at the online measurement, the only differences being the amount of powder transported through the system and the unknown particle delivery device (Taghavivand, 2021). However, the machine ran for approximately 1 minute per test – and the results only show around a quick spike of voltage around 10 seconds before returning to 0v. One possible reason was due to the charged powder initially leaking from the top and coating the outside of tube and grounding the metal clips used to collect charge. Even with the data collected, none of the graphs showed consistent results. Another reason that the graphs were not able to be consistent was due to the charge not being directed through the connections towards the amplifier, but rather to any location on the charge measurement system that was not grounded. This meant that the whole system needed to be re-evaluated and any section not properly grounded needed to be reconnected to grounding wires. With all these issues

stemming from the initial design of the online charge measurement system, a new set-up using the offline charge measurement methods was decided upon.

In addition, electrical issues caused this design to be unfeasible. The loose powders not collected by the Faraday cup would obtain charge and cause shocks along the surface of anything not grounded. This caused electrical failures in the amplifier, oscilloscope, and mass balance.

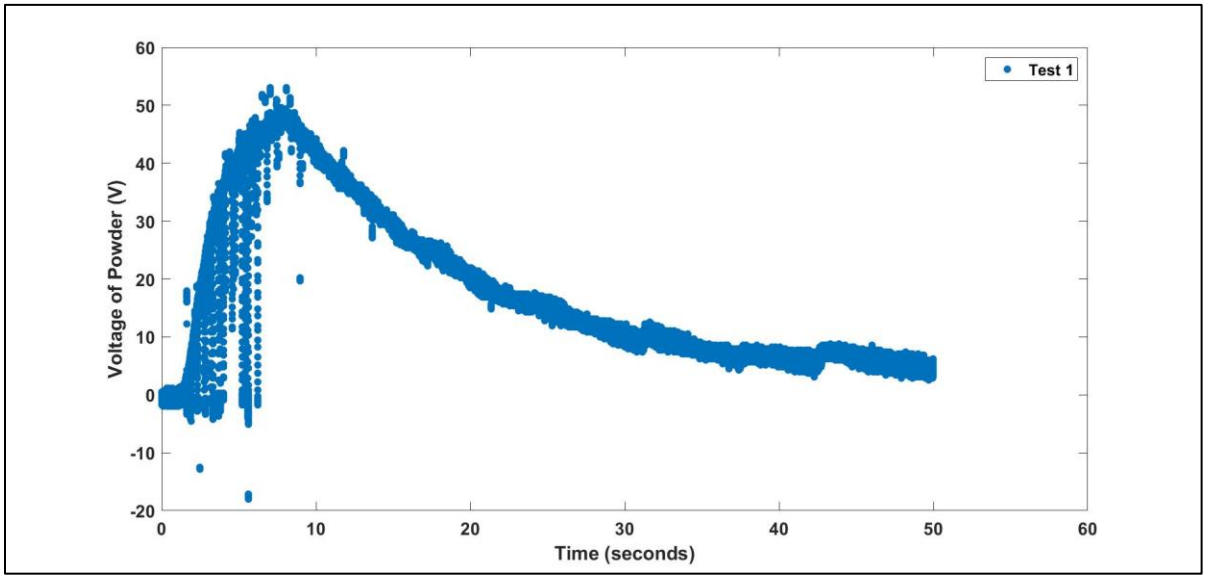

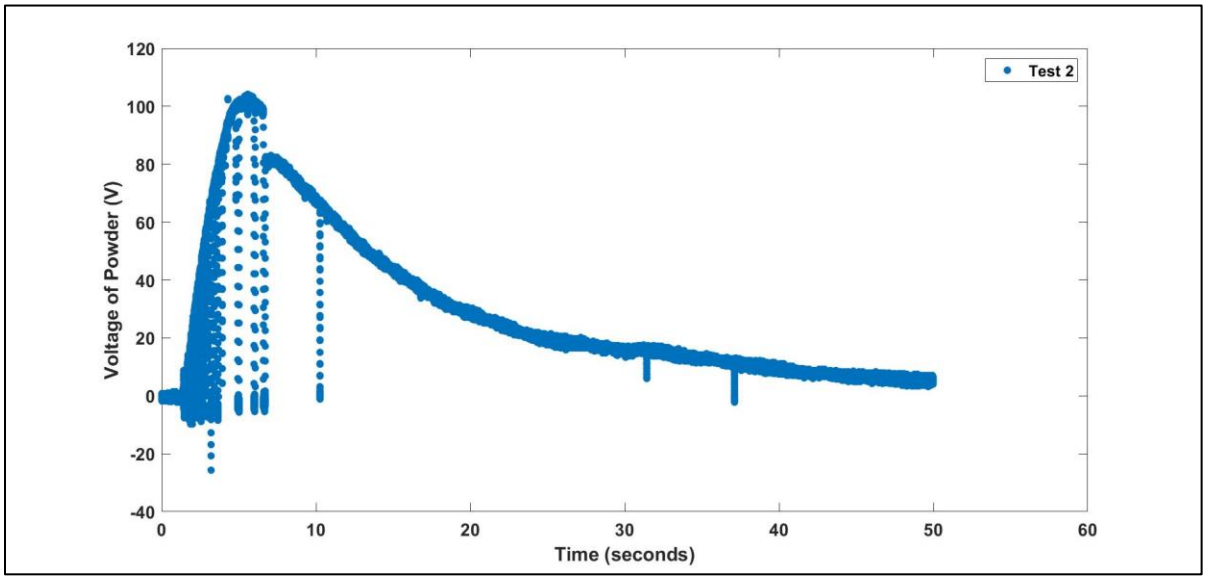

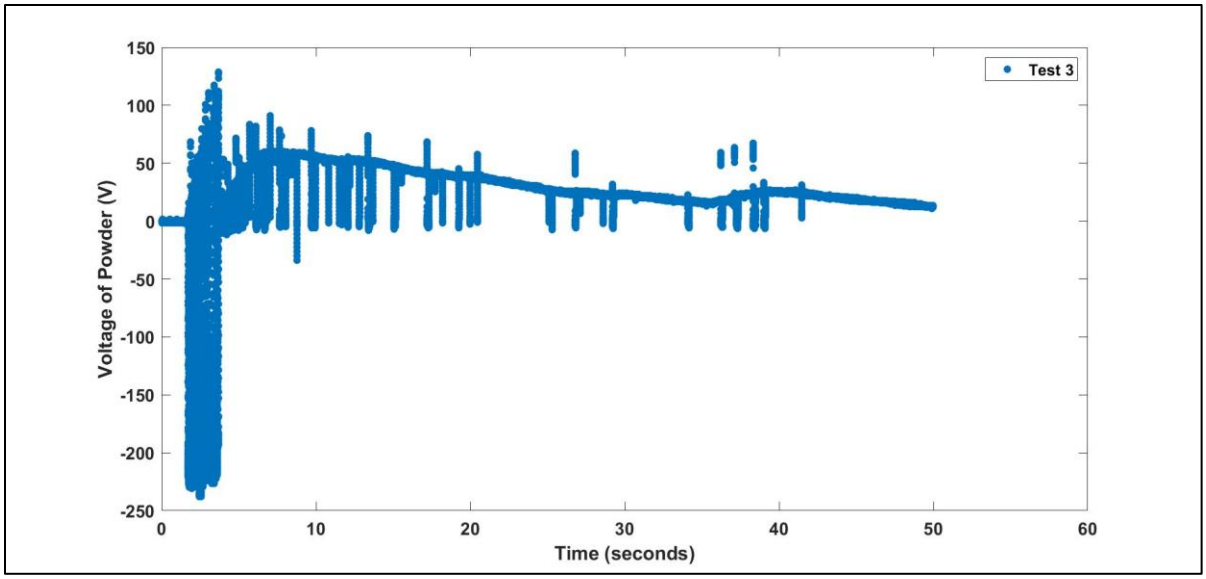

Figure 15 a-c. Three graphs of initial online charge measurements.

4.4. Charge Measurement Design #2

The offline measurement system was completed, and initial tests were run with undried and dried wheat flour. After confirmation that the machine could produce consistent results, other powders were introduced into the system such as chickpea flour, milk powder, soymilk powder, and soy protein. After pure powder trial runs had been completed as a baseline test, particle size, airflow, powder mixture ratios, and protein content were analyzed and compared in respect to the charge-mass ratio of the particles.

4.4.1. Pure Powder Charges

Initial tests were run using undried wheat flour, results can be seen in Table 2. The table indicates a charge-to-mass ratio average of 1.9538 µC/g, which the charge averaging 2.8375µC and the mass being 1.4429g. These are believed to be acceptable results, as the standard deviation between is quite low at 0.08525. The results from Table 2 were plotted and can be seen in Figure 16. The graph shows a linear relationship for the mass of the particles and the charge of the particles, this means that the charge mass ratio should remain

within the same range. In addition, specifically at the mass of 1.3g – there appears to be some variation in the charge. While this should be the same charge at the same mass this could be due to the powder not being dried and having moisture retained in the particles causing less accurate results. Additional tests were also completed using chickpea flour, soymilk powder, milk powder, and soy protein. To eliminate error coming from moisture content within the powder, all pure powders were re-tested except for milk powder. Milk powder was not dried, as the process of drying the powder was possibly too harsh and caused it to burn and be unusable. Results for both dry and undried pure powders can be seen in table 3 and Figure 17.

Table 2. Initial Charge-Mass Ratio Test with Undried Flour

Trial	Mass in Hopper (g)	Air Flow (LPM)	Vibration Level	Time (minutes)	Net Final Mass (g)	Final Charge (μC)	Charge-Mass Ratio (μC/g)
1	10	15	5	4	1.4	2.688	1.92
2	10	15	5	4	1.9	4.008	2.1095
3	10	15	5	4	1.7	3.449	2.0288
4	10	15	5	4	1.5	2.892	1.928
5	10	15	5	4	1.3	2.5	1.9231
6	10	15	5	4	1.3	2.418	1.86
7	10	15	5	4	1	1.907	1.907
						AVERAGE	1.9538
						STD. DEVIATION	0.08525

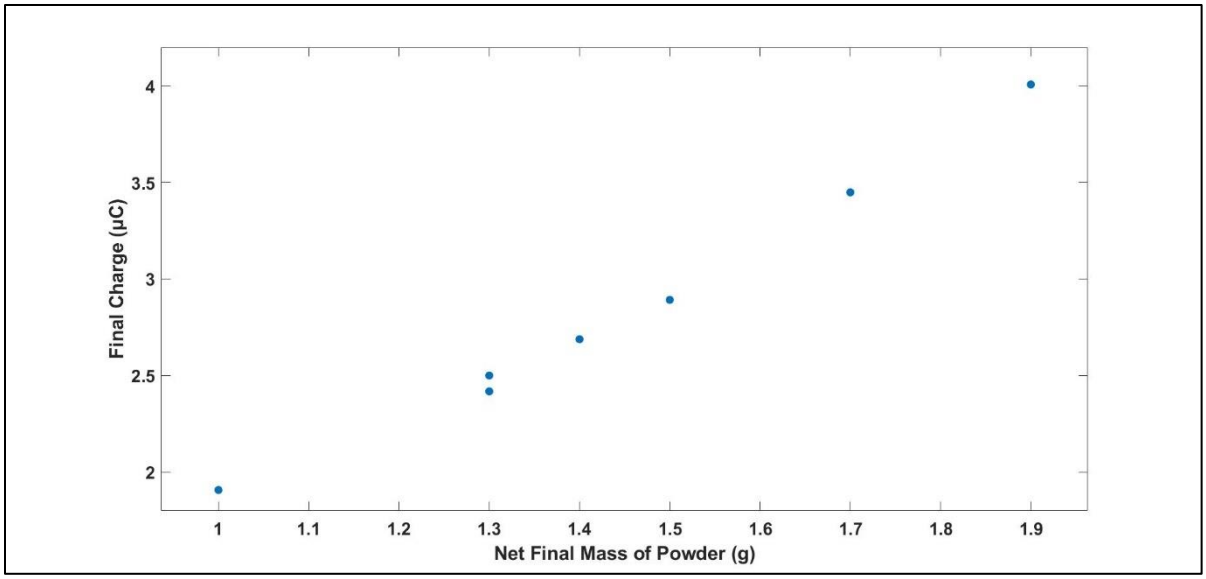

Figure 16. Graph of final net mass of the undried flour within the Faraday cup and the respective charge in micro-coulombs.

Table 3. Pure Dried and Undried Powders Charge-Mass Ratio

Undried Pure Powders				
Powder	Initial Charge Directly in Cup (µC)	Net Mass (g)	Final Charge (µC)	Charge-Mass Ratio (µC/g)
Wheat Flour	-0.0002	1.4429	2.8374	1.954
Chickpea Flour	0.0008	1.4667	9.582	6.540
Soymilk Powder	0	1.3833	6.6248	4.815
Milk Powder	0.0005	1.6125	3.778	2.312
Soy Protein	0.0003	1.933	14.311	7.649
Dried Pure Powders				
Powder	Initial Charge Directly in Cup (µC)	Net Mass (g)	Final Charge (µC)	Charge-Mass Ratio (µC/g)
Wheat Flour	-0.0002	3.45	8.248	2.4462
Chickpea Flour	0.0008	1.0833	8.208	7.593
Soy Milk Powder	0	2.9	15.909	5.483
Soy Protein	0.0003	0.9333	7.8667	8.437

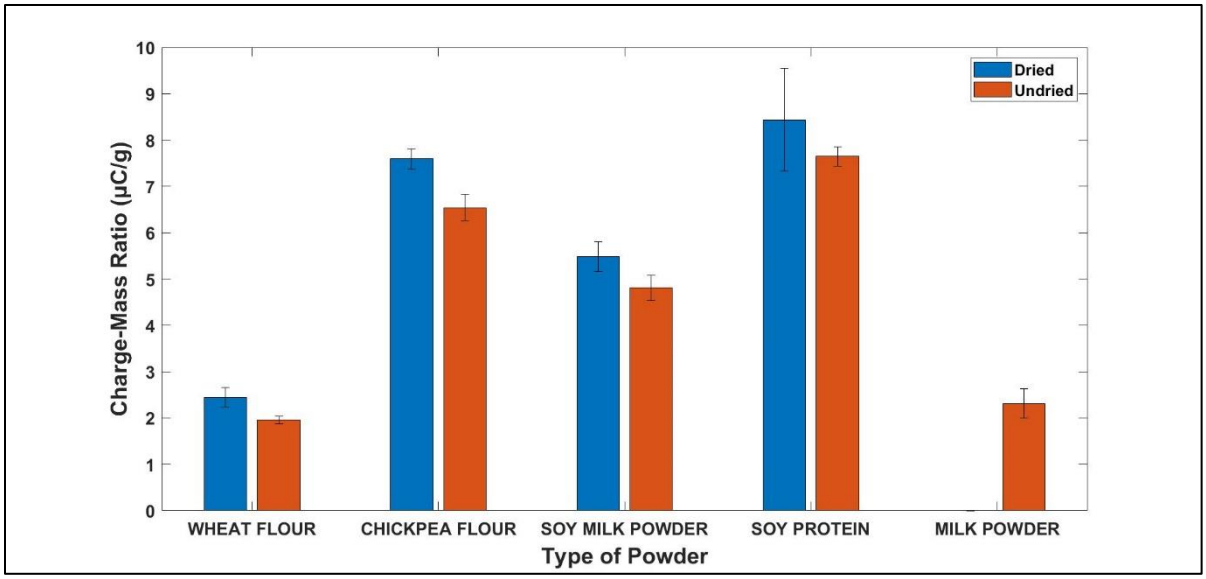

Figure 17. Pure Powders Dried and Undried Charge-Mass Ratios of Wheat Flour, Chickpea Flour, Soymilk Powder, Soy Protein, and Milk Powder

Looking at results obtained from both the dried and undried flour, there is an increase in charge-mass ratio when the powder is dried. This is due to moisture being removed from the powder as it is dried. When water is absorbed into the powder, the surface resistivity decreases causing charge reduction. Vice versa, when the water is removed from the powder in the form of drying, the surface resistivity increased in turn causing a greater charge. This has been cited by both Rezende et al. in their research on charge distribution in insulator surfaces and Karolina et al. in their research of the surface chemistry and humidity of electrostatic powders (Rezende et al., 2009 and Korlina et al., 2017). Another reason the charge-mass ratio of the dried powder is greater than undried powder is the flowability of the dried powder resulting in a larger mass being collected and a greater charge-mass ratio. Badawy et al. wrote about pharmaceutical wet granulation; within the research they talk about the negative impact water absorption or wet powder has on flowability. This is due to multiple reasons such as bridging powders to inhibit free movement or degrading material

quality (Badawy, 2019). From the trials completed, all dried powders have larger charge-mass ratio than the undried powder, confirming both theory and results.

4.4.2. Half-Half Compositional Powder Charge

To visualize the charge of a powder with a compositional mixture of 2 powders, chickpea flour and wheat flour was mixed as a ratio of 25:75, 50:50, and 75:25. Trail runs were completed, and the results can be seen in the table 4. Figure 18 shows the charge-mass ratio of wheat flour, chickpea flour, and the mixture ratios graphed for comparsion.

Table 4. Charge, Mass, and Charge-Mass Ratios of Mixture for Wheat and Chickpea Flour

Initial Mixture Ratio (Chickpea Flour: Wheat Flour)	Final Mixture Ratio from Protein Content Tests	Net Mass (g)	Final Charge (μC)	Charge-Mass Ratio (μC/g)
100:0	100:0	1.0833	8.208	7.5930
25:75	36:64	2.5000	6.4216	2.6082
50:50	63:37	1.0714	3.911	3.4933
75:25	70:30	1.3667	6.2433	4.6734
0:100	0:100	3.4500	8.248	2.4462

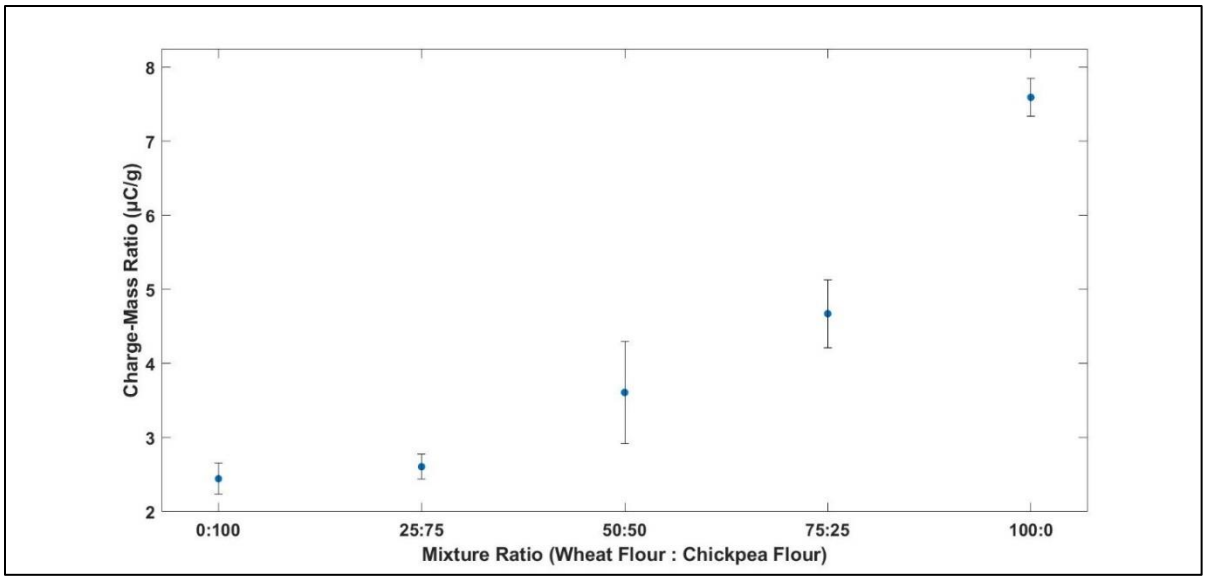

Figure 18. Charge-mass ratio of wheat flour, chickpea flour, and 50-50 mixture.

The results shown in Figure 18, show that the 50:50 mixture has a mass-charge ratio within the range set by wheat and chickpea flours. Normally results would determine direct correlation as seen with research completed, for example Anderson and Fox who not only studied the effect of two powders being mixed but also chose to go one step further and analyze 3 mixed powders using mathematical equations determined that the charge of the powder mixture would be directly proportional to the ratio of powders mixed (Anderson & Fox, 1995). However, the real-time experiment 50:50 mixture charge-mass ratio isn't exactly half-way in between the two charge-mass ratios of the pure powders. Possibly, a larger amount of the wheat flour ended up in the Faraday cup rather than the chickpea flour. Since the wheat flour has a lower charge-mass ratio if the end mixture in the faraday cup has more wheat than chickpea – the charge-mass ratio will be lower. In addition, the 75:25 mixture is not halfway between the 50:50 mixture and pure chickpea flour, this could be due to the same reasoning mentioned above. To see if the hypothesis was correct, protein tests were completed on the mixture ratio.

Results for the mixture ratio found through the protein content tests can be seen in table 4., while the final mixture ratios were not exactly the expected values, the values were very close – there was not a high discrepancy. This makes it hard to then say there was an imbalance of the expected ratio causing a non-linear set of results as shown. In fact, going of the mixture's ratios collected, each ratio had a higher amount of chickpea flour then intended. Seeing as chickpea flour has a higher charge-mass ratio then all the mixture ratios should be higher than their expected value, but instead results show a lower charge-mass

ratio than expected for all mixtures. Therefore, the hypothesis above would not be able to explain the charge mass ratio of the powder mixtures.

Another more likely hypothesis that would explain the discrepancy in the expected results of charge-mass ratio would be the possibility of coagulation between particles. The belief is that the pure wheat and chickpea flour do not stay separate and aggregate as the particles get transported from the fluidized bed to the Faraday cup where the charge is measured. When particles coagulate or aggregate, their surface properties can change, which can influence their charge distribution and behavior. This could be due to the contacting surfaces being exposed to new chemical environment that change the surface chemistry of the particles, additional ion absorption from surrounding environment altering the charge distribution and enhanced electrostatic interactions between the proximity of the coagulated particles. The hypothesis that the coagulated particles influence the charge or fluidization of the particles more than the individual pure powders can be backed-up by research completed by Hakim et al. on the characteristics of fluidized aggregates of nanoparticles within a fluidized bed, the same method of particle transportation used in this thesis. The results indicated that the properties of the aggregated or coagulated particles had a greater influence on the minimum fluidization velocity within the fluidized bed rather than the primary nanoparticles individually (Hakim et. al, 2005). As previously discussed with better fluidization, the charge-mass ratio or charge per particle should increase, therefore an effect from the coagulated particles would be noticed.

4.4.3. Sifted Powder Particle Size

To see the effect of particle size of the charge, chickpea flour was sifted using different size ranges and trials were run, seen in table 5.

Table 5. Sifted Chickpea Flour Size Ranges and Charge-Mass Ratio

Size Ranges (μm)	Net Mass (g)	Final Charge (μC)	Charge-Mass Ratio (μC/g)
38-60	0.1333	0.9740	7.410
90-106	0.5333	3.5710	6.7139
125-150	0.5333	3.3147	6.2145

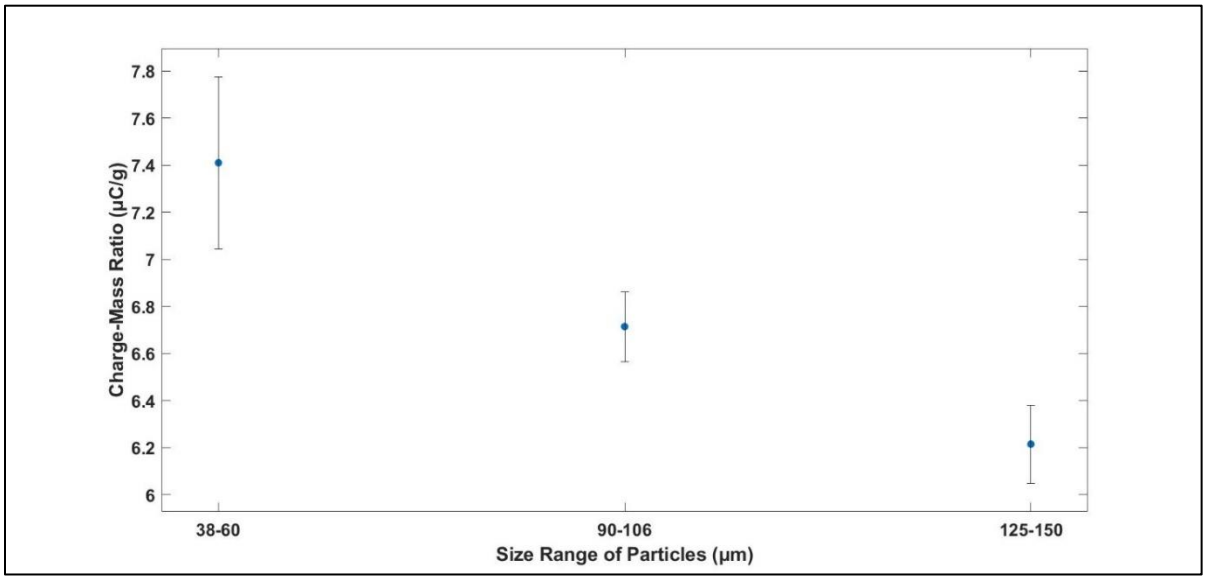

Figure 19. Sifted Chickpea Flour Size Ranges vs. Charge-Mass Ratio

Looking at table 5 and Figure 19. Sifted Chickpea Flour Size Ranges vs. Charge-Mass Ratio which depicts a graphed comparison of the particle sizes vs. charge-mass ratio, as the size of the particle increases the charge of the particle decreases. This can be due to multiple theories. The first possible reason the results show an increase in charge-mass ratio with the decrease in particle size could be due to the fact that large particles are generally governed by their inertia, while smaller particles can depend on both turbulent effect and inertia of

particles. Mehrtash explained that larger particles respond to changes in turbulent streamline flow, as their response time is much higher than the turbulent time scale due to a high Stokes number. Meanwhile, smaller particles have lower Stokes numbers – this can result in them either completely following the streamlines and creating minimum interaction with the surface wall or the particles can have just enough inertia where they can collide with the wall but not enough to remain on the center turbulent streamlines, resulting in repeated collisions with the surface material until exiting the tube (Mehrtash, 2021). Therefore, the smaller particles will have more collisions with the wall, while larger particles remain within the streamline flow and not collide with the surface material as much.

Another reason for the difference in charge-mass ratio could be chickpea flour is made by grinding up chickpeas, therefore the particles are not uniformly made. Each particle is not identical as some are protein bits and others are the shell or other starch particles (Samira, 2021). Seeing as the protein particles are smaller and are known to have a higher charge, when the powder becomes sifted the larger shell particles are removed leaving protein particles mostly. This would in turn cause a higher charge-mass ratio. Results from protein content testing confirm that the highest protein content for size ranges came from the smallest size range, confirming this theory and results.

4.4.4. Effect of Airflow

Airflow was examined to determine whether there could be an optimal airflow and to see if it had an effect on the charge. Milk powder was used for the trials and airflow was changed from 5-25 LPM in increments of 5LPM. Reynolds number was calculated for each airflow to

determine whether the flow in all cases would be laminar, turbulent, or intermediate. Results can be seen in table 6 and the graph displayed in Figure 20.

Table 6. Effect of Airflow on Charge-Mass Ratio of Milk Powder

Airflow (LPM)	Reynolds Number (Laminar or Turbulent)	Net Mass (g)	Final Charge (μC)	Charge-Mass Ratio (μC/g)
5	2204.70 (Intermediate)	0.15	0.1878	1.229
10	4409.39 (Turbulent)	0.5	0.6911	1.458
15	6614.09 (Turbulent)	1.613	3.778	2.312
20	8818.78 (Turbulent)	3.871	7.306	1.889
25	11023.48 (Turbulent)	2.367	6.201	2.612

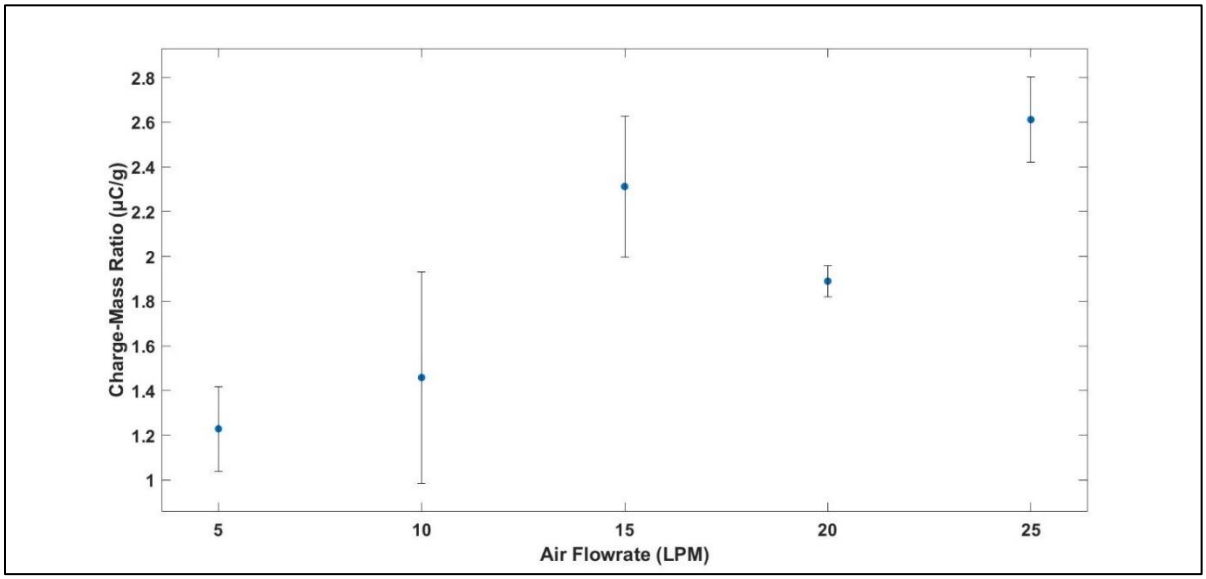

Figure 20. Airflow of Milk Powder vs. Charge-Mass Ratio

Two plausible factors affecting airflow can be the phase of airflow (laminar, mixed, or turbulent) and the impact in which the particles are hitting the contact surface. An increase in airflow would create an increase in impact of the particles hitting the surface material. As

stated in work completed by Matsuyama and Yamamoto, as particles hit the surface material, the particles have a greater direct impact of force. They found the normal forces created by the particles were proportional to the charge and determined that as the normal force of impact increases, the charge of the particles increases as well (Matsuyama and Yamamoto, 1994). As shown in the results above, as the air flow rate increases from 5 to 15 and onwards to 25 the charge-mass ratio increases which could be due to the impact force of the particles.

Due to the error bar, there is no, statistical significance difference between the results at 5 and 10 LPM while there is significance difference between 15 and either of 5 or 10. In addition, the 20 LPM results show a decrease in charge-mass ratio, not following this trend. The state of airflow being turbulent or laminar could possibly be used to explain this. Mehrtash explains in his report that more particle-wall interaction occurs in lower air velocity, whereas in higher air velocity, particles barely collide with the pipe wall before exiting the pipe. Therefore, the particle collision at 5 LPM should be larger than at 10 LPM, and 15 LPM should have larger collision numbers than 20 LPM. The greater charge-mass ratio should be a result of larger collision numbers, so the charge-mass ratio at 10 LPM and 20 LPM should be lower than 5 LPM and 15 LPM respectively. Mehrtash also hypothesizes that higher airflow shows an increase in charge could come from the smaller particles passing through high air velocities trapped at the center eddies of the pipe flow and exit the pipe before gravity force pulls them towards the pipe wall. So, the charge in the test runs completed in this thesis show an increase as the airflow increases from 5 LPM to 25 LPM, but certain airflows like 10 LPM and 20 LPM show a slight decrease which could be due to the decrease in collision numbers (Mehrtash, 2021).

It is important to note that no optimal airflow working for every powder can be determined. As mentioned above, different powders have various factors that affect the flowability. Seeing as every powder tested is different, they will all have different values given to those external factors that affect flowability, for example bulk density, frictional values, etc. (Lee et. al, 1998). This can change the flowability of the particles and also how much powder is needed to coat the surface of the inner faraday cup without having over saturation.

4.4.5. Effect of Protein Content

SEM results can be seen in the photos organized in figure 21. The figures below show the size of the particles at 20 and 100µm. Using the photos below, average size distribution was calculated using surface area mean, the values can be seen in table 7. After calculations, soy protein and flour had the largest particle diameters at approximately 24 and 21 microns respectively, while soymilk powder had the smallest particle size of approximately 11 microns. To display the full array of the of the particle diameter sizes per particle type, histograms from the size distribution data collected from the SEM photos has been displayed in Figure 22. The nutritional content of each powder's, protein, and carbohydrates can also be seen in table 7.

Magnification Level	100µm	20µm
Milk Powder	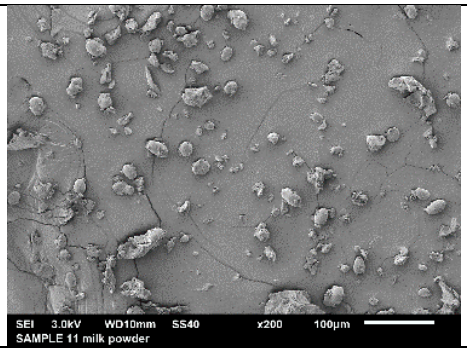	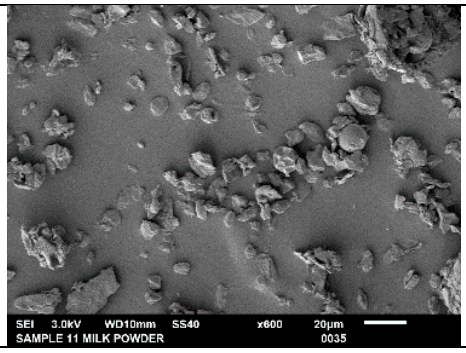

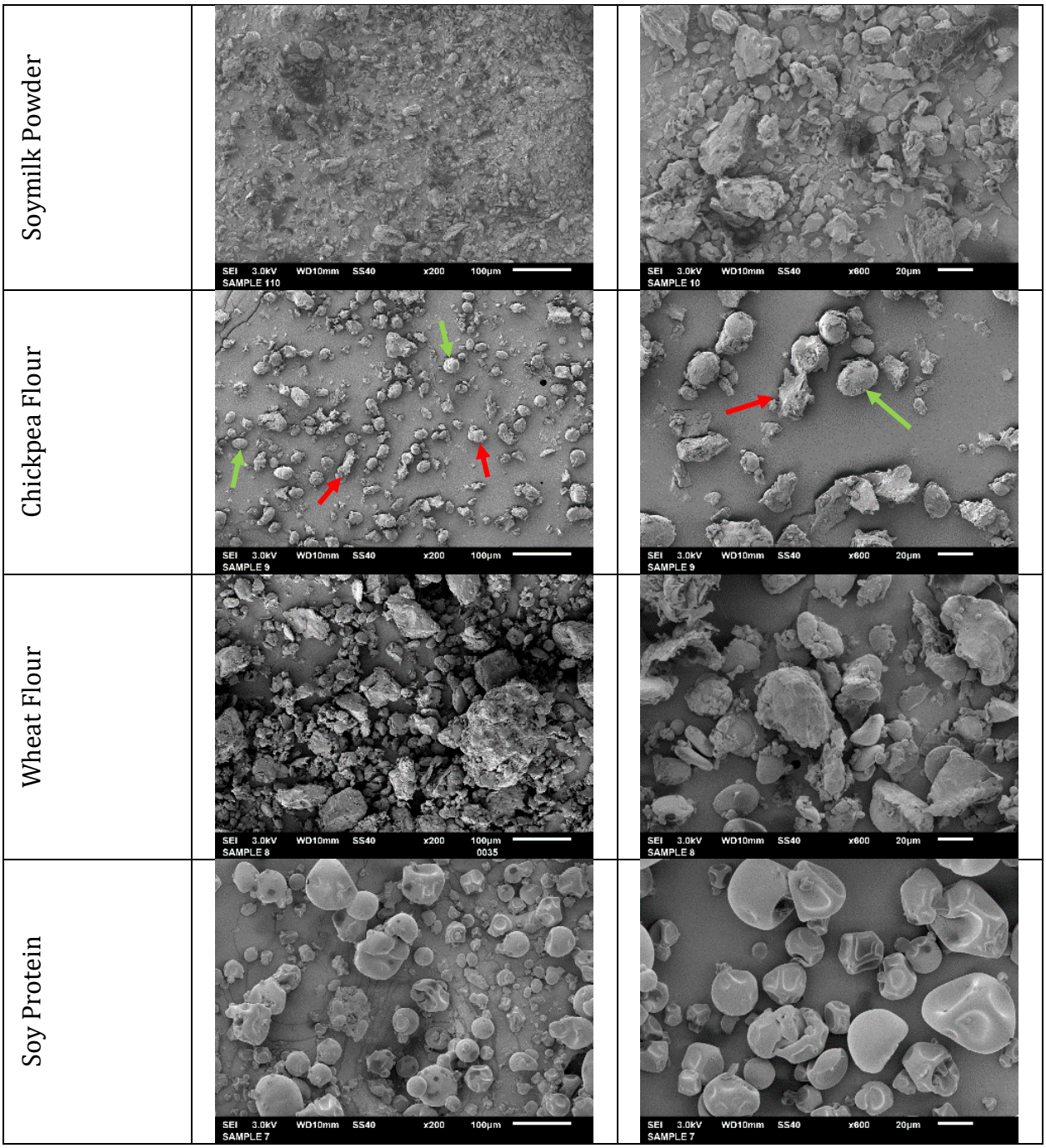

Figure 21. SEM particle distribution photos for all pure powders taken at 20 and 100 micrometers. Arrows on the chickpea 20- and 100-micron magnification photos are used to identify the various types of particles within the flour. The red arrows indicate proteinaceous matrix and fibrous particles, while the green arrows indicate starch granules.

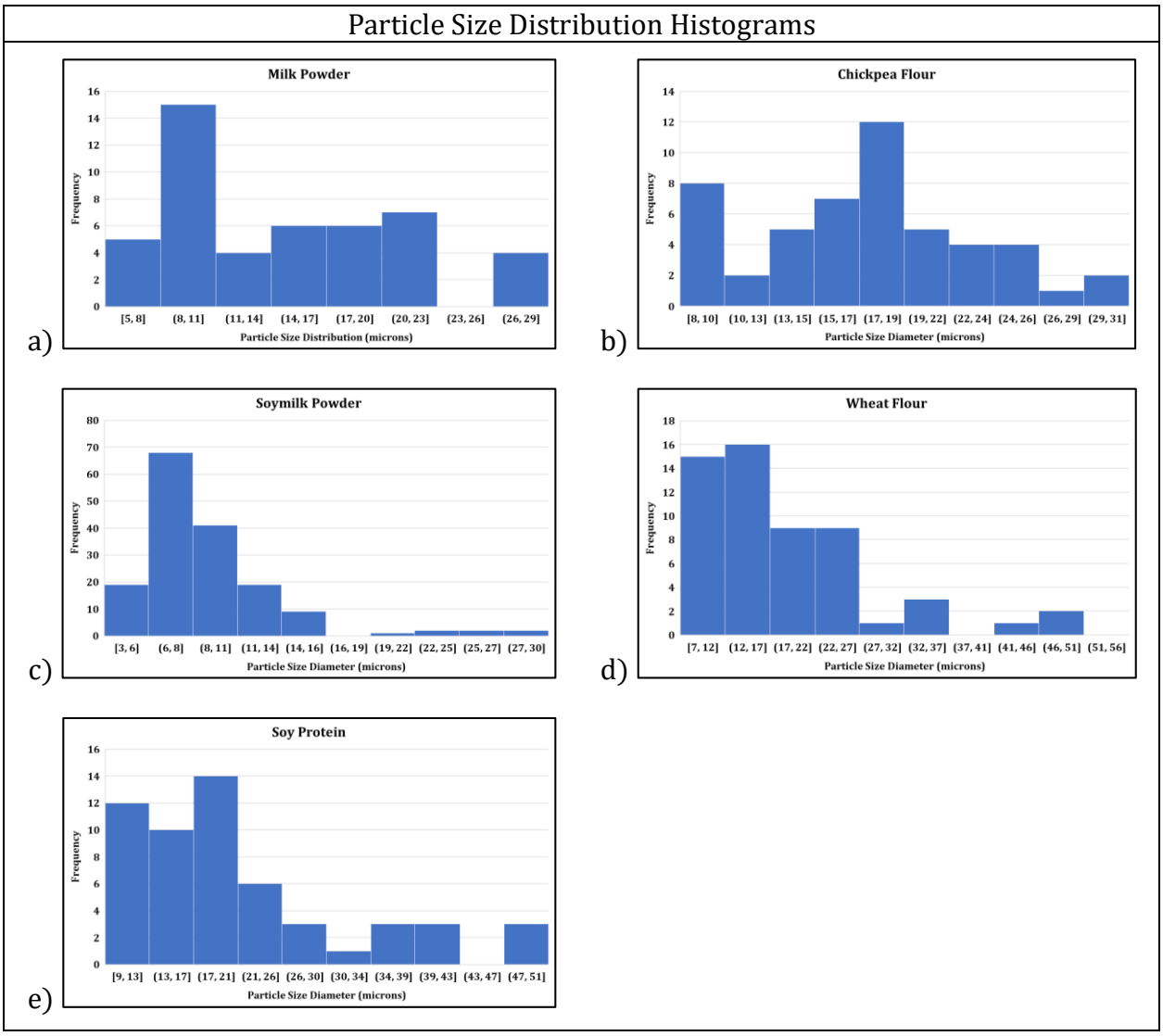

Figure 22. Size distribution histograms from the diameter measurements obtained from the SEM graphs in figure 21. The graphs are in the following order: a) milk powder, b) chickpea flour, c) soymilk powder, d)wheat flour, and e) soy protein.

Table 7. Nutritional Content (Carbohydrate, and Protein) of Powders Used in Charge-Mass Ratio Experiments and the Mean Diameter of Particle Size found from SEM Photos

Type of Powder	Mean Diameter of Particles (μm)	Protein (wt%)	Carbohydrate (wt%)
Wheat Flour	21.725	13.3333	70
Chickpea Flour	18.053	22	58
Milk Powder	16.703	26.9	38
Soymilk Powder	11.182	51	35
Soy Protein	24.294	26.9	38

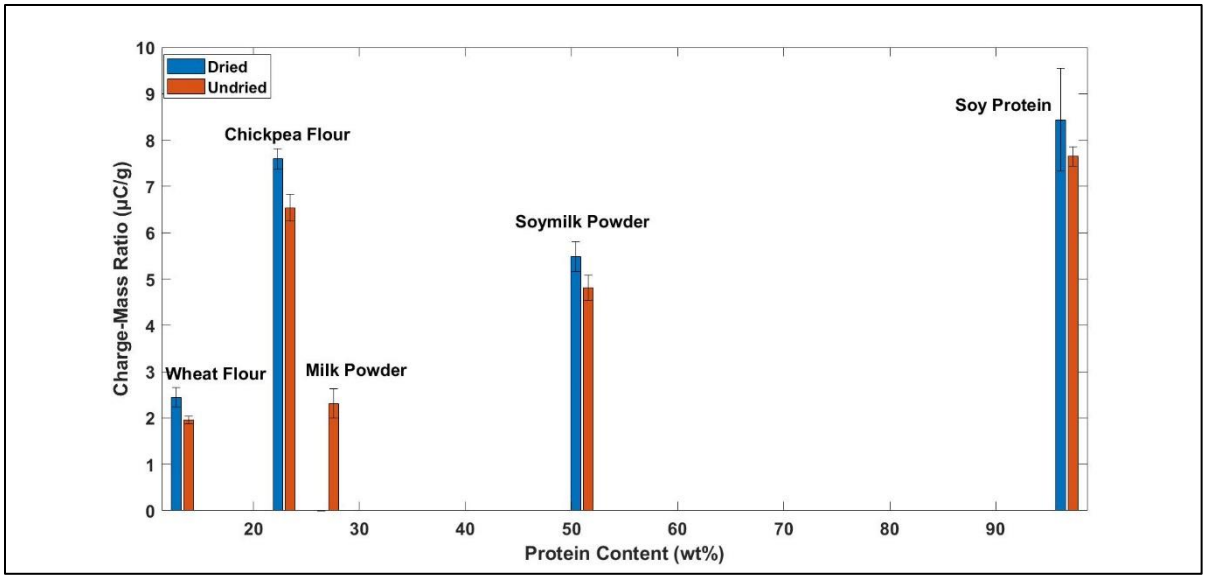

Figure 23.Protein Content (wt%) vs. Charge-Mass Ratio of Dried and Undried Pure Powders

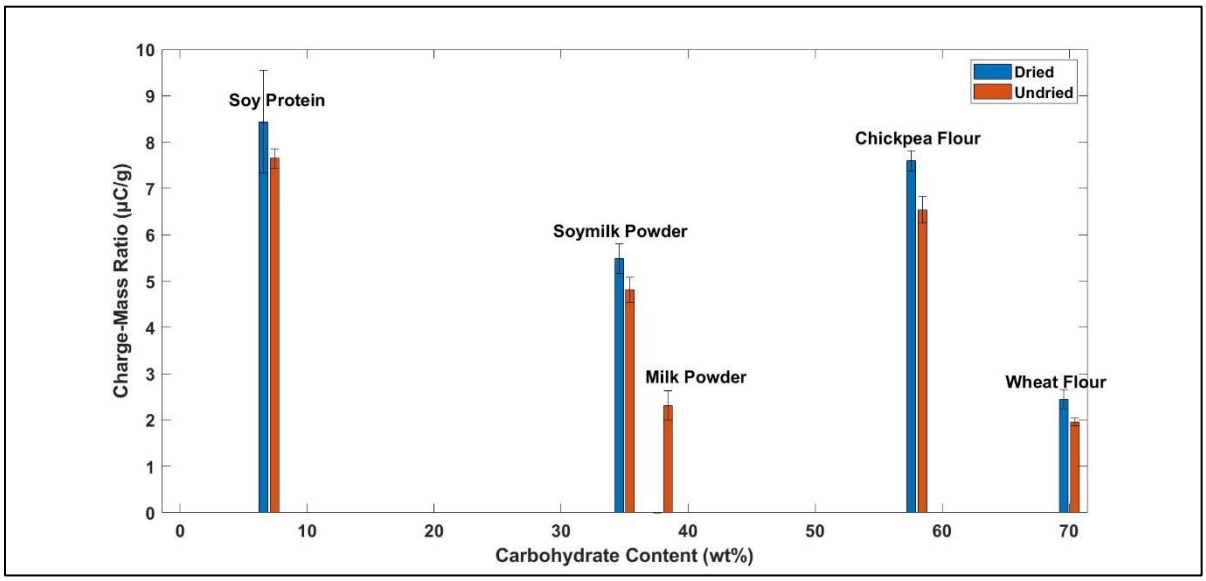

Figure 24. Carbohydrate Content (wt%) vs. Charge-Mass Ratio of Dried and Undried Pure Powders

Nutritional content was compared to the charged of the dried and undried powders, seen in figure 23-24. There does not appear to be a correlation between the charge of the particles and the carbohydrates of the particles. Protein content shows that as the protein weight percent (wt%) increases, the charge-mass ratio of the powders increases, however this is

not consistent throughout all the powders used in the trial runs – as the chickpea flour does not fit this trend. The protein increasing proportionally with charge-mass ratio is the expected results, as research completed by Mehrtash showing computational and mathematical results depicted that the relationship between protein content and charge-mass ratio obtained would be directly proportional (Mehrtash, 2021). In addition, Landauer and Foerst completed a study on particle contact number with tribocharging and the effect protein content has on the separation process. The paper concluded the higher the protein content, the higher the contact potential (which means higher work function) and therefore with two particles of the same size, the particle with higher protein content will receive higher charge transfer compared to the other particle of the same size with lower protein content (Landauer and Foerst, 2019).

The chickpea results not fitting this trend could possibly be due to the density and size of the particles, as it shown above that both factors can affect the charge-mass ratio. Size distribution tests for all the pure powders were completed, it was concluded that soymilk powder had a mean diameter of 18 microns with the other pure powders ranging from 11-24 microns. Seeing as the chickpea flour had the median average diameter size of the particle type sizes, it could be determined that the size of the particle most likely did not contribute to the charge-mass ratio being an outlying point.

Looking at the SEM image of the chickpea powder in detail arrows have been used to indicate which particles in the chickpea flour are proteinaceous matrix, fibrous particles, and starch granules. The starch granules have been identified using the green arrows and resemble a circular shape with no hard edges. The fiber and protein particles have more rigid and sharp

shapes, examples can be seen identified with the red arrows (Tabtabaei et. al, 2019). In addition, looking at the SEM pictures of different particles, the chickpea particles are more round or circular in comparison to other particles like wheat flour and soymilk which are flatter and more rigid. Particle shape can play a significant role in determining powder flowability. Irregularly shaped particles can lead to interlocking, arching, and other flow impediments that result in poor flow behavior. Spherical or regular particles, on the other hand, tend to exhibit better flowability due to reduced interlocking tendencies and smoother interactions. As mentioned above, the flowability of the particles plays a large role in varying the charge-mass ratio. Research to support the hypothesis that particle shape plays a key-role in varying the charge per particle was completed by Rezaei et. al who researched how size, shape and density of biomass particles influence their transportation, fluidization, rates of drying and thermal decomposition. The biomass used for this research was pellet particles with a more circular shape and chip particles that have a more rectangular shape. Results concluded that the pellet particles are less likely to aggregate to each other and will flow easier than the chip particles. This identified that circular particles had better fluidization than particles with more rigid edges. In addition, the research found that the shape or morphology of the particles affected the flow properties more than the particle size (Rezaei et. al, 2016). The spherical particles (chickpea and soy protein) have greater capabilities in fluidization, and a greater charge-mass ratio, therefore it is hypothesized that the morphology or shape of the particle plays a key role in effecting charge. In addition, the particles for chickpea appear to be predominately smaller particles rather than larger chunks all clump together. This would also result in better fluidization, as the larger chunks would be harder to fluidized due to the greater mass of the particle. Seeing larger chunks in

both soymilk and milk powder, this could explain why the soymilk powder has a smaller charge-mass ratio than chickpea flour, which should not be the case if a larger protein content results in a greater charge-mass ratio.

Results for this analysis show that not only does particle size, distribution, and shape play key roles in determining charge-mass ratio of particles, but particle shape is more influential than particle size.

Chapter 5. Mathematical Modelling

To compare experimental results, mathematical modelling was completed to obtain the work functions of the powders.

For the math modelling to be successful, appropriate collision values had to be obtained for each particle type. Factors that would affect the collision number would be particle shape, particle size, type of airflow (laminar/turbulent), shape of airflow pathway, and coagulation of particles. While calculating the mean collision number would provide more accurate results within the math modelling to account for all the variables mentioned above; obtaining exact equations, research articles, and theoretical background that was necessary was found to be out of the scope and timing for this project. The mean collision number was determined by comparing the mean collision numbers found in a research paper written by Matsusaka. The velocity and pipe length was approximately the same as the values used in the real time experiments completed in section 4, therefore the mean collision number obtained in the paper, 3, was used as an estimate value (Matsusaka et. al, 2002). Future research will have to be completed to obtain exact collision numbers to display mathematical modelling more accurately.

The efficiency of charging also had to be calculated in order to obtain the contact potential difference. Matsuda formulated an equation to solve for collision number and can be rearranged to solve for the efficiency of the charging, as seen in equation 15.

$$k = \frac{\pi D_{particle}^2}{2Sn_0\left(1 + \frac{3m\rho_{air}D_{pipe}\bar{u}}{4m\rho_{particle}D_{particle}\bar{v}}\right)} \tag{15}$$

A diagram showing how equation 6 from section 2 and equation 15 are being implemented is shown using the flowchart in figure 26. The mathematical modelling was carried out for each individual pure powder, the calculated values can be seen in table 8.

Figure 25 a-b. a) Flow chart for math modelling of work function of particles and charge-mass ratio and b) Replica of flow chart equations in place of word description for variables.

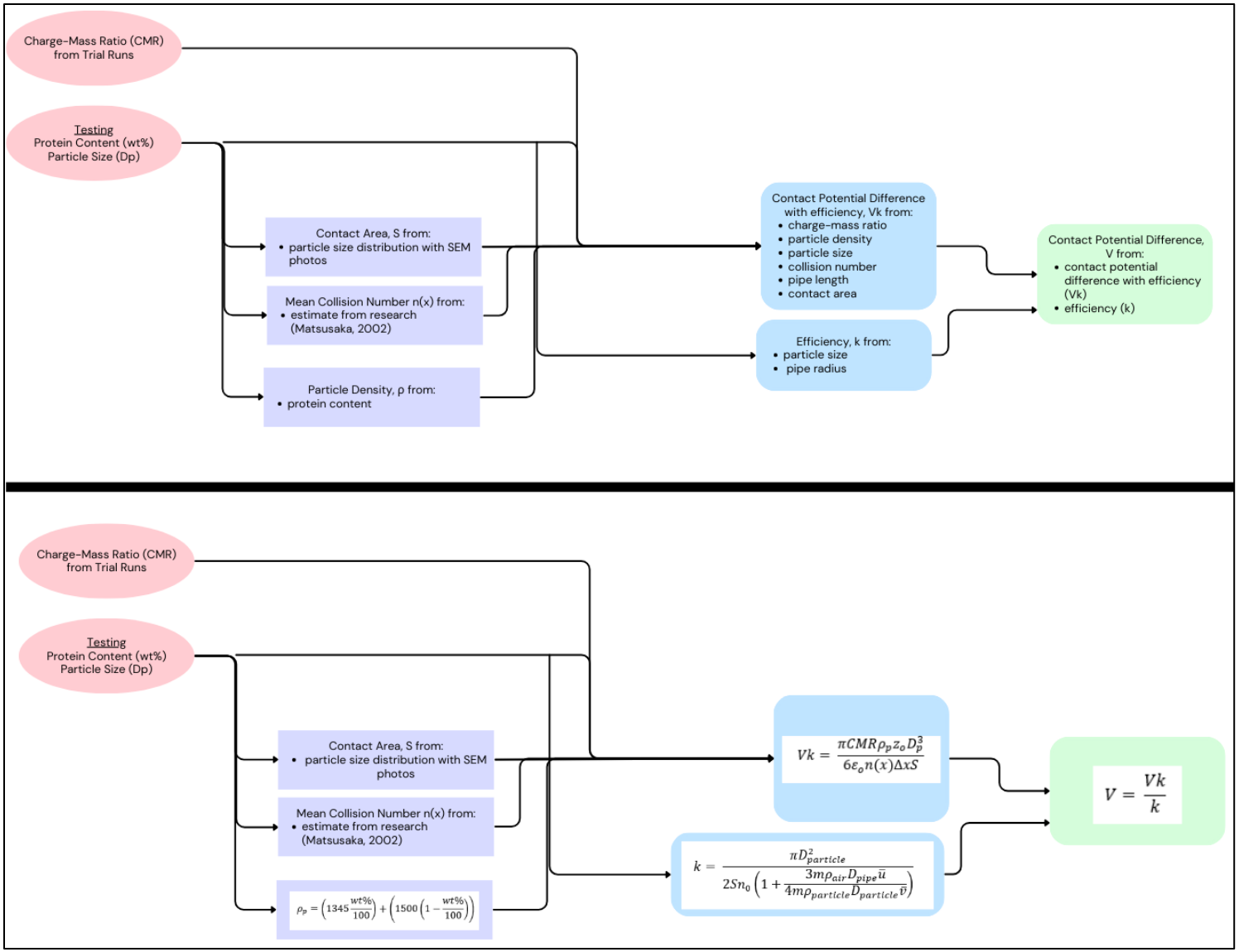
Charge-Mass Ratio (CMR) from Trial Runs
Testing
Protein Content (wt%)
Particle Size (Dp)
Contact Area, S from:
• particle size distribution with SEM photos
Mean Collision Number n(x) from:
• estimate from research (Matsusaka, 2002)
Particle Density, ρ from:
• protein content
Contact Potential Difference with efficiency, Vk from:
• charge-mass ratio
• particle density
• particle size
• collision number
• pipe length
• contact area
Efficiency, k from:
• particle size
• pipe radius
Contact Potential Difference, V from:
• contact potential difference with efficiency (Vk)
• efficiency (k)
Charge-Mass Ratio (CMR) from Trial Runs
Testing
Protein Content (wt%)
Particle Size (Dp)
Contact Area, S from:
• particle size distribution with SEM photos
Mean Collision Number n(x) from:
• estimate from research (Matsusaka, 2002)
$\rho_p = \left(1345\frac{wt\%}{100}\right) + \left(1500\left(1-\frac{wt\%}{100}\right)\right)$
$Vk = \frac{\pi CMR\rho_p z_o D_p^3}{6\varepsilon_o n(x)\Delta x S}$
$k = \frac{\pi D_{particle}^2}{2Sn_0\left(1+\frac{3m\rho_{air}D_{pipe}\bar{u}}{4m\rho_{particle}D_{particle}\bar{v}}\right)}$
$V = \frac{Vk}{k}$

Table 8. Mathematical Modelling Results for Pure Powders, Sifted Size Ranges, and Flour Mixture Ratios

Pure Powders						
Powder Type	Particle Size	Protein Content, wt%	Experimental Charge-Mass Ratio (μC/g)	Mean Collision Number	Charging Efficiency, k (eq. 15)	Contact Potential Difference (V)
Wheat Flour	21.725	13.3	1.95	3	8.56×10^{-2}	6.78×10^{-6}
Chickpea Flour	18.053	22	6.54	3	9.25×10^{-2}	2.20×10^{-5}
Milk Powder	16.703	26.9	2.31	3	7.21×10^{-2}	7.21×10^{-6}
Soymilk Powder	11.182	51	4.82	3	4.37×10^{-2}	1.62×10^{-5}
Soy Protein	24.294	96.7	7.65	3	8.56×10^{-2}	3.45×10^{-5}

The mathematical modelling shows a linear relationship between the contact potential difference and charge-mass ratio, where both will increase with respect to each other. This can be seen in Figure 26, where soy protein can be seen as having the highest charge-mass ratio and contact potential difference. Inversely, the wheat flour has one of the lowest charge-mass ratios and contact potential difference. Looking at the particle-to-wall collision modelling done by Matsuda (equation 6 from section 2.4) as the contact potential difference increases, the charge-mass ratio should increase additionally. This can be seen in other research written by Trigwell et al. In the literature they studied the tribocharging of coal versus other minerals for separation and used work function as one of the ways to discern a change. When looking at the results, things such as surface oxidation/contamination,

humidity and other external factors that are also factors of tribocharging charge-mass ratios were factors changing or transforming work function (Trigwell et al., 2001).

In addition, Figure 26 also displays the protein in wt% beside each data point, the modelling also shows a linear relationship between protein content and contact potential difference, with the exception of chickpea flour. As stated above in section 4.4.5. possible reasons for this outlying powder type could be size and shape of the particle.

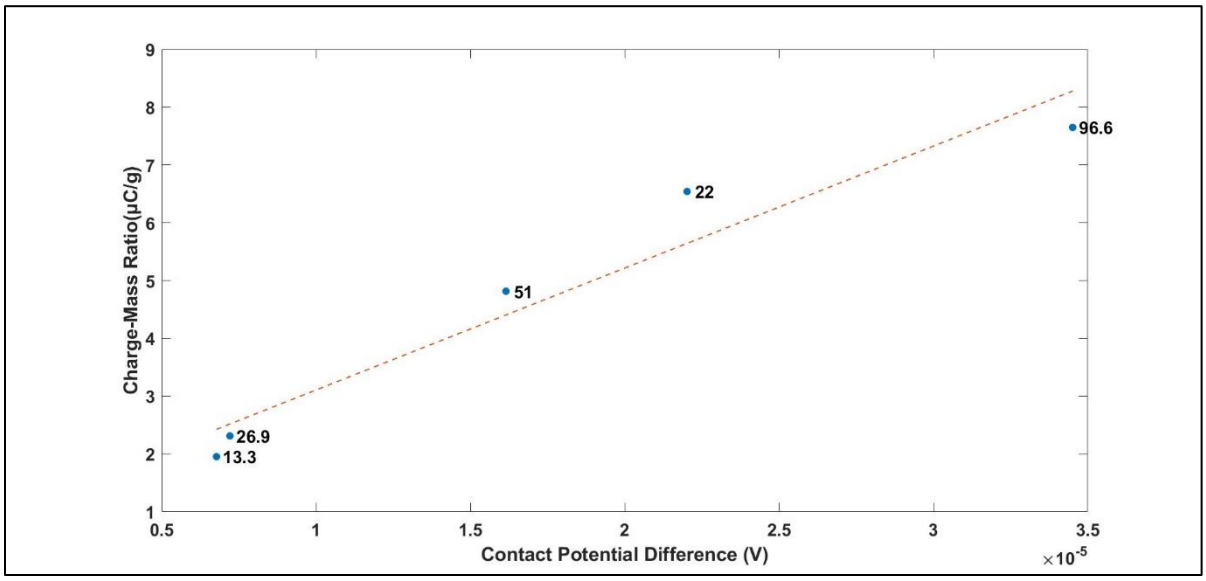

Figure 26. Graph displaying relationship between calculations of contact potential difference from math modelling and undried pure powder charge-mass ratios. The wt% of protein content for each powder type is present beside the data point.

Removal of the chickpea flour was completed and results for both contact potential difference and charge-mass ratio were analyzed. As shown in Figure 27, both contact potential difference and charge-mass ratio increase proportionally as the protein content increases. This matches the data collected and research articles mentioned in previous sections, confirming results obtained by the real time experiments.

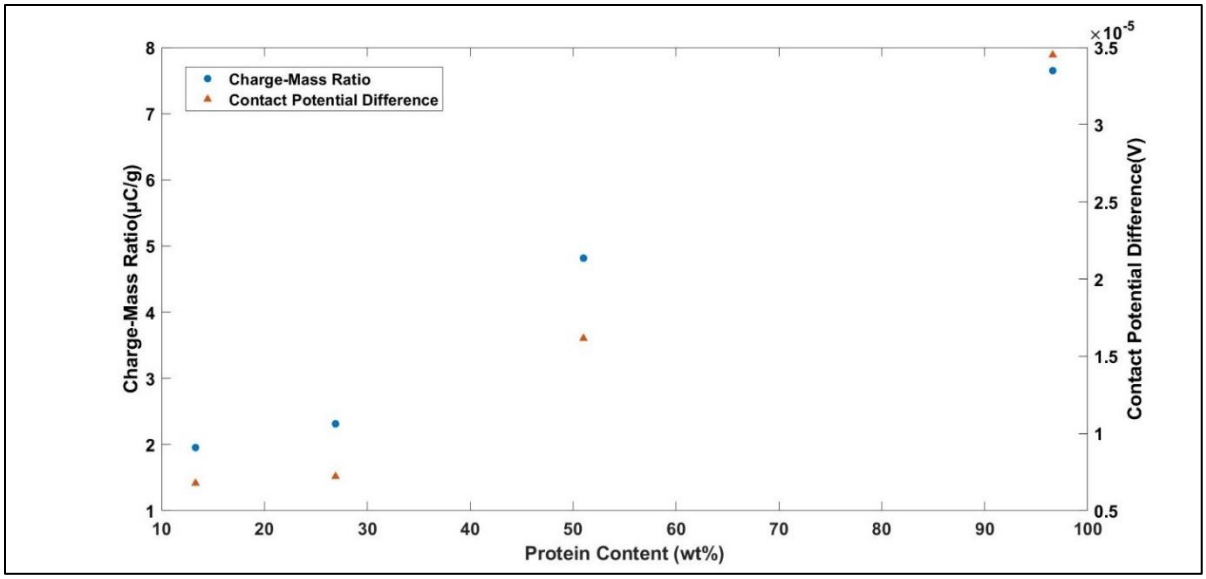

Figure 27. Graph displaying protein content (wt%) vs. charge-mass ratio and contact potential difference with the removal of outlying data point (chickpea flour).

As of current time, no new conclusions can be drawn from the mathematical modelling. With future work including a calculated collision number, the effect of particle charge on contact potential difference and work function could be completed.

Chapter 6. Conclusions and Future Work

The objective of this thesis was to create a system that had consistent mass delivery and tribo-charge measurement. This was with the purpose of running tests with multiple food-grade powders and analyzing the chemical/physical make-up of the powders and their relation to the protein content of the particles. There was 3 different mass delivery systems designed and created. The current mass delivery system is able to constantly provide transport of the powder particles, however it is not able to confirm consistent flow rate for the particle delivery. For charge measurement, an online and offline system had been designed to collect the charge of the particles. The currently used set-up for trials was the offline system, as the online was not able to be fully sealed and had the capability to cause electrical failures.

Trial runs were executed with the current offline mass delivery and charge measurement system, and environmental factors such as particle size, mixture ratios, airflow rate, and protein content were compared and analyzed. After running tests conclusions have been made.

- Dried powder creates a higher charge-mass ratio than undried pure powders, due to the flowability of the powder creating a higher mass and the removal of moisture decreasing the electrical resistivity of the powders.
- Particles with smaller diameter sizes have a higher charge-mass ratio than particles with a larger mean particle size. Theories for why this would occur include the effect of turbulent flow vs. inertia, a greater number of particles resulting in a greater

collision number, or reduction of surface area causing the charge collected per surface area to be more concentrated or greater.

- Powder mixtures will have a charge-mass ratio in between the range of the initial pure powders mixed. In addition, as the amount of powder with a higher charge-mass ratio increases, the charge-mass ratio of the whole mixture will increase. While the initial belief was the relationship should be linear, the coagulation or aggregation of particles cause variances in the charge-mass ratio.
- As airflow increases, charge-mass ratio increases, due to influences of impact force of particle and collisions numbers caused by the turbulent airflow pathways. It should be noted, there is no optimal or "set" airflow.
- Particle protein content is directly proportional to charge-mass ratio, as the protein content increases, the charge-mass ratio increases. Chickpea flour was an outlying powder type that did not fit the relationship, due to particle size and shape. From this data however, it was concluded that particle shape was more influential in charge per particles, than particle size.

Mathematical modelling was also used to determine the effect of the work function for the particles. It was concluded that as the charge-mass ratio increased, the contact potential difference increased respectively. In addition, it was seen that as the protein content increased, the contact potential difference increased respectively. Explanations for both results had already been mentioned in the real time experiments, and seeing as these results as well were already anticipated, no new conclusions could be drawn from the math modeling.

In conclusion, tribocharging can be seen as a dangerous process when it comes to safety in certain machine operated work environments. But, in industries such as the pharmaceutical, automotive, and more notably the food industry – tribocharging can be seen to have massive benefits and create smooth-operating processes. In order for this to occur it is important to note the effects of the physical and chemical properties that could affect the powders used in the tribocharging process.

Further research should be conducted to determine the effects of humidity on tribo-charging and how it can be correlated with protein content results or other environmental factors. Another external factor to be tested would be acidity and basicity to determine functional groups within powders and then correlate them with charge. In addition, calculations to find the exact mean collision numbers for different particles and their external factors could result in more accurate or precise modelling for the effect of particle charge on contact potential difference and work function could.

Chapter 7. Appendix A

7.1. 3D CAD Drawings

Figure 28. 3D CAD drawing of auger used in the screw feeder for mass delivery design 1.

Figure 29. 3D CAD Drawing for bottom half of screw feeder and hopper for mass delivery designs 1 and 2.

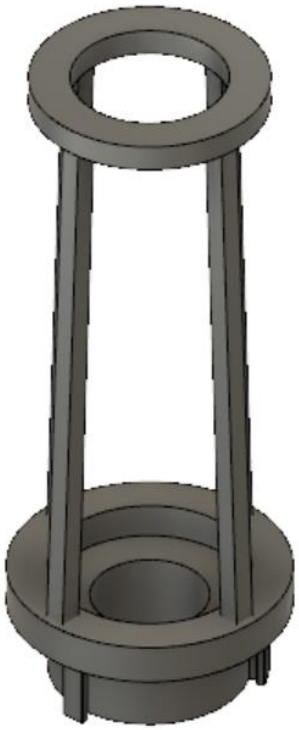

Figure 30.3D CAD drawing of hopper holder used for mass delivery design 1.

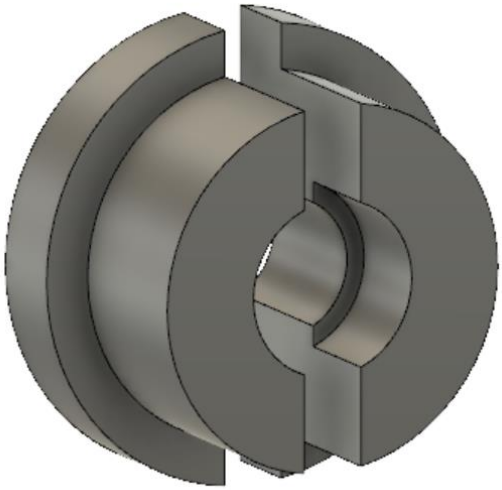

Figure 31. 3D CAD drawing for the hopper holder used for mass delivery design 2 and 3.

Figure 32. 3D CAD drawing for tube used for connection to screw feeder and the hopper in mass delivery design 1 and 2.

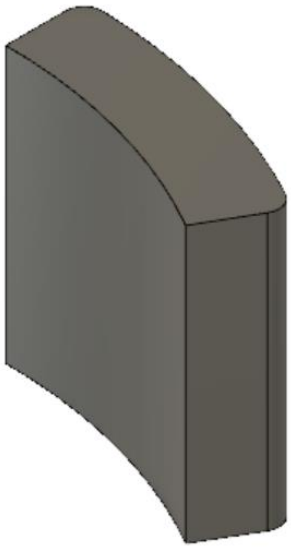

Figure 33. 3D CAD drawing or spacers on the current charge measurement container used to attach clasps.

Figure 34. 3D CAD drawing of the bottom and top lids for the charge measurement design 2 container used to hold the Faraday Cup.

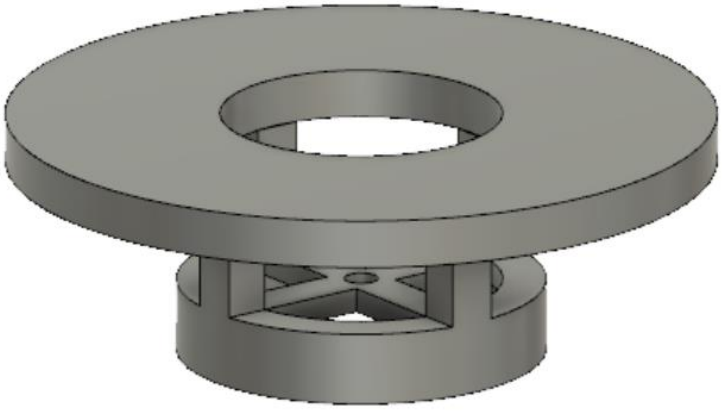

Figure 35. 3D CAD drawing for lid used on Faraday cup for charge measurement design 1 and 2.

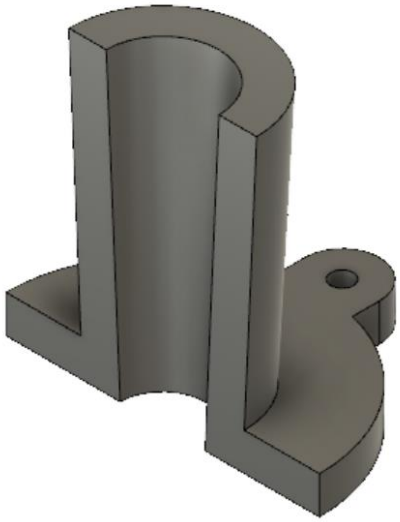

Figure 36. for addition to figure 30's container top used to allow access to the cable connected to the Faraday Cup

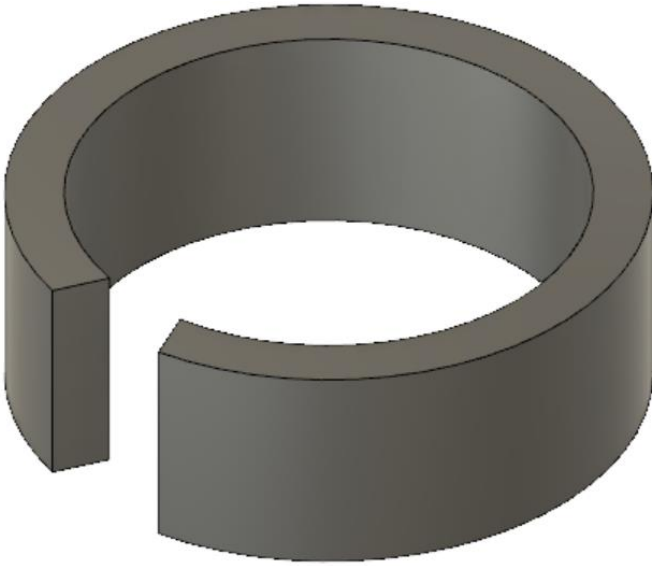

Figure 37. for a sleeve used to provide an airtight seal to the Faraday Cup lid shown in figure 30. This is used in tandem with figure 34, spacers connected to the sleeve.

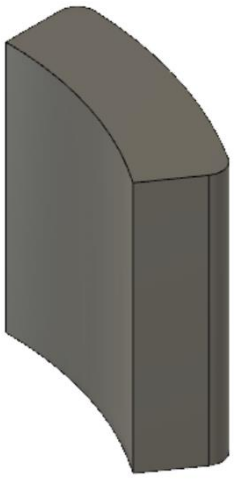

Figure 38. 3D CAD drawing for spacers attached to faraday sleeve (figure 33). Used to provide airtight seal to Faraday Cup and Faraday Cup lid (figure 31).

Figure 39. 3D CAD drawing for connection for hopper to tube used in mass delivery design 3.

Figure 40. 3D CAD drawing for hopper lid with connection to airflow used in all mass delivery designs. The addition of the O-ring cutout was only inputted in design 3.

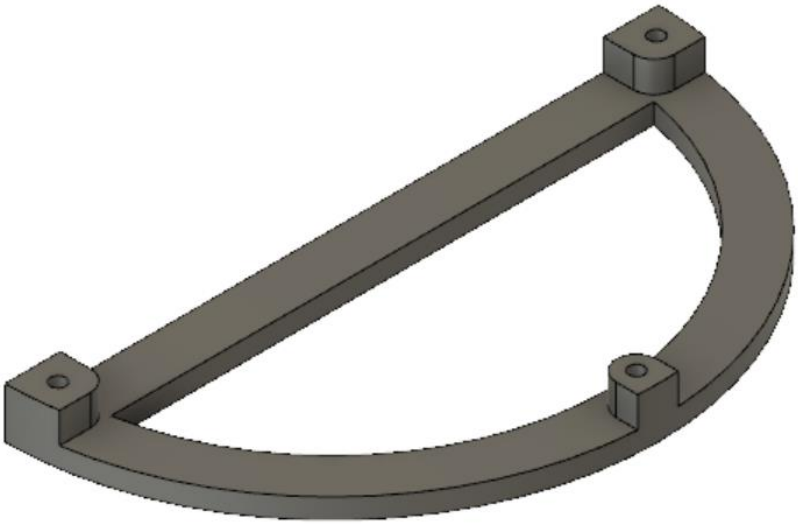

Figure 41. 3D CAD drawing for filter lid used on the top of the mass delivery container lid (figure 30). Used to allow air to escape the container.

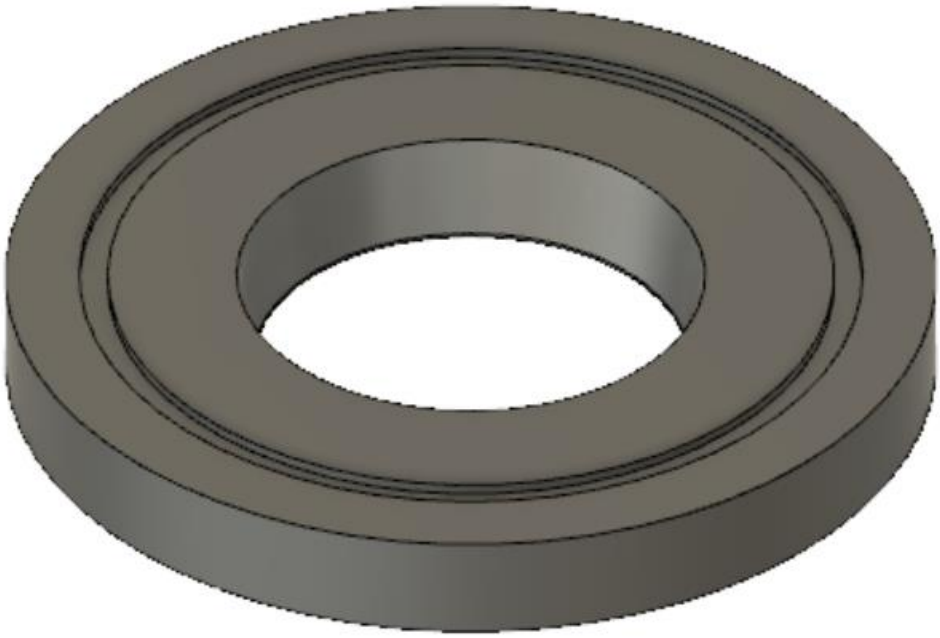

Figure 42. 3D CAD drawing for opposite side of the hopper lid (figure 36), used to provide an airtight seal. This was designed for mass delivery system 3.

7.2. Manufacturing 2D-Drawings for Parts

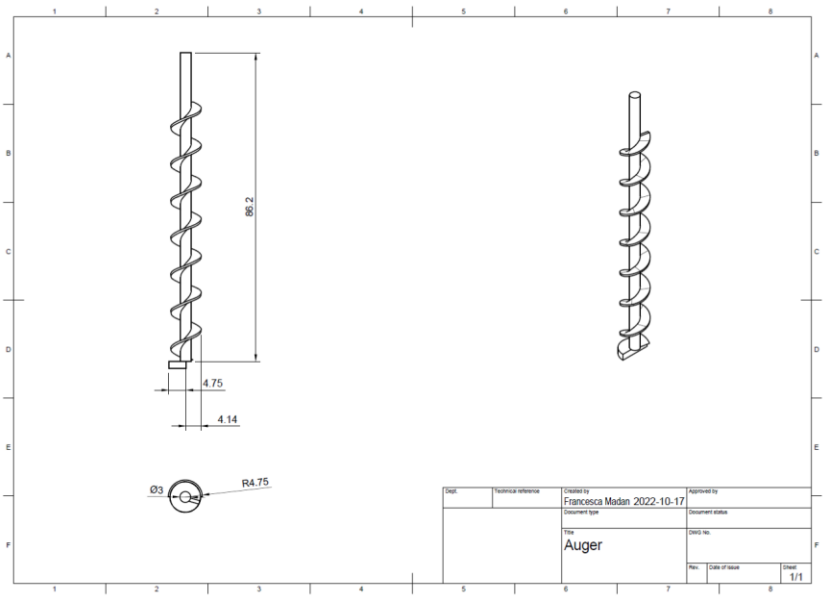

Figure 43. Manufacturing 2D-drawing of auger used in mass delivery design 1.

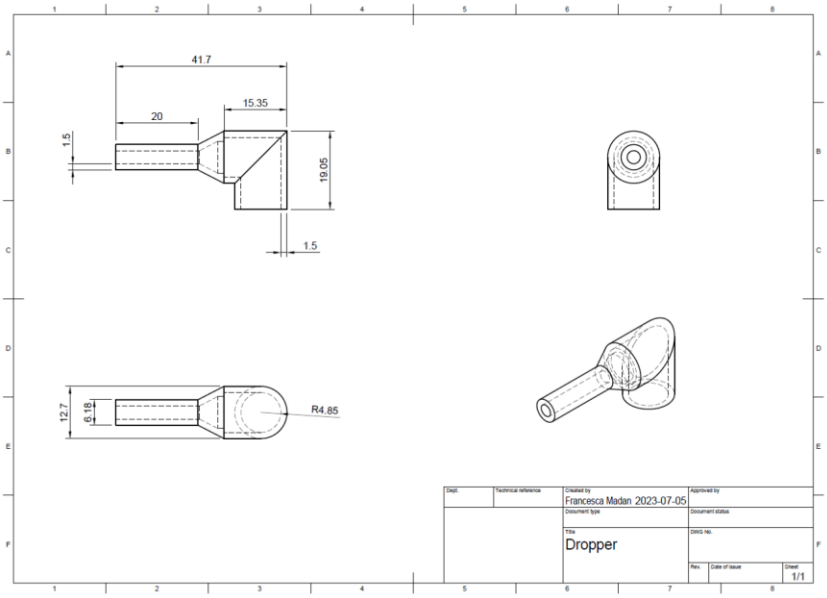

Figure 44. Manufacturing 2D-drawing for bottom half of screw feeder and hopper for mass delivery designs 1 and 2.

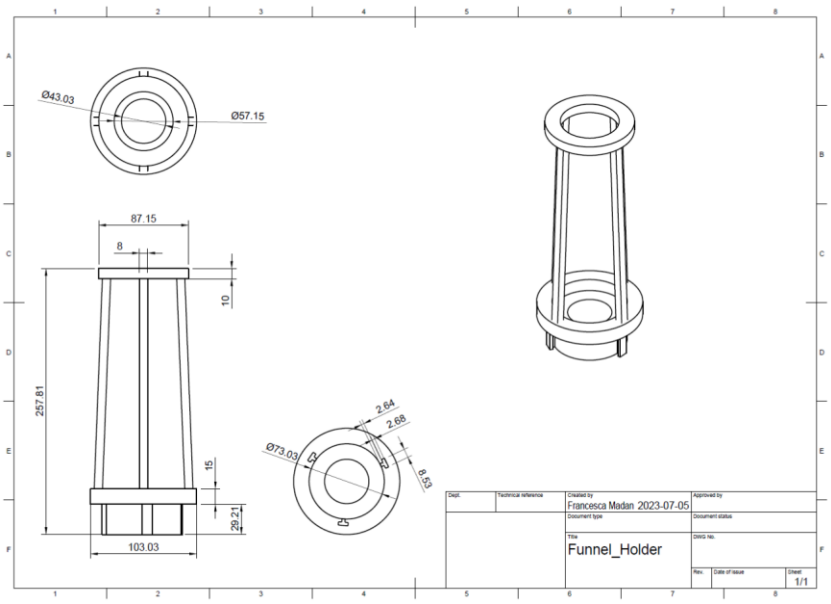

Figure 45. Manufacturing 2D-drawing of hopper holder used for mass delivery design 1.

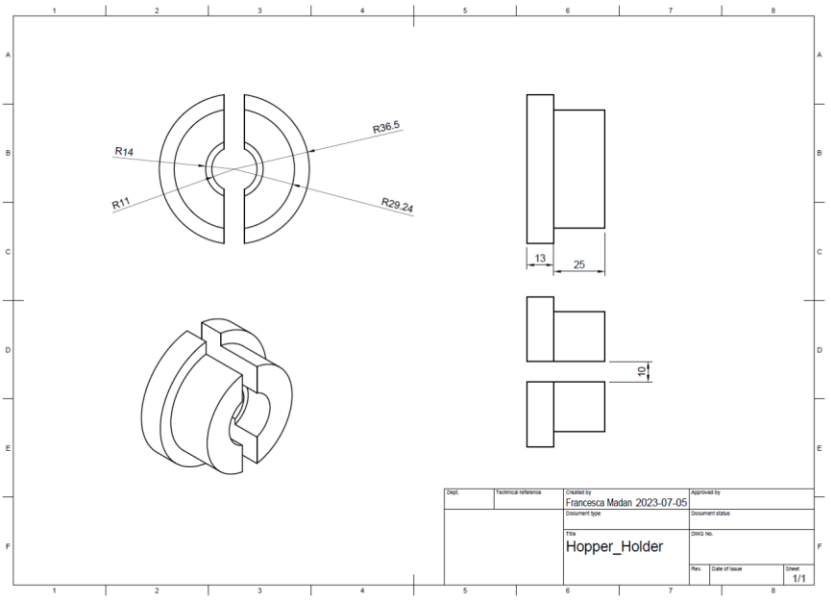

Figure 46. Manufacturing 2d-drawing for the hopper holder used for mass delivery design 2 and 3.

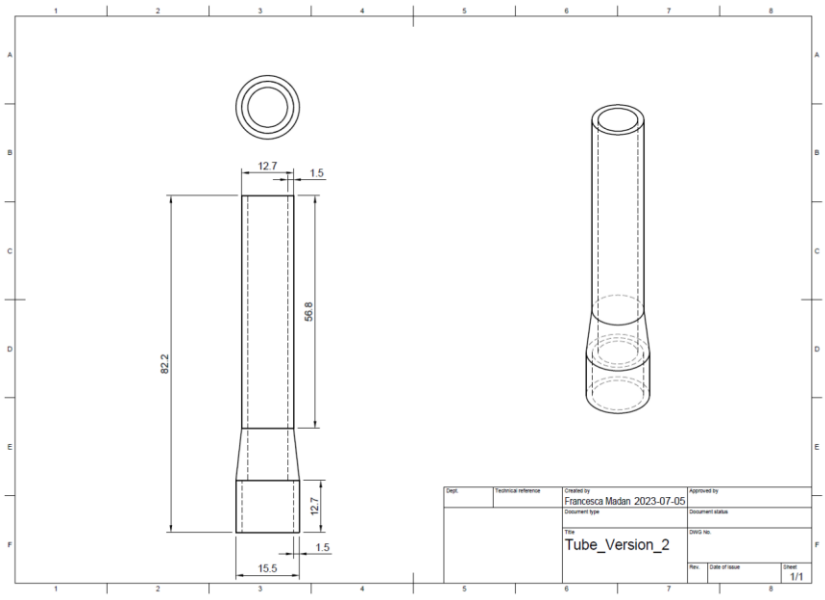

Figure 47. Manufacturing 2D-drawing for tube used for connection to screw feeder and the hopper in mass delivery design 1 and 2.

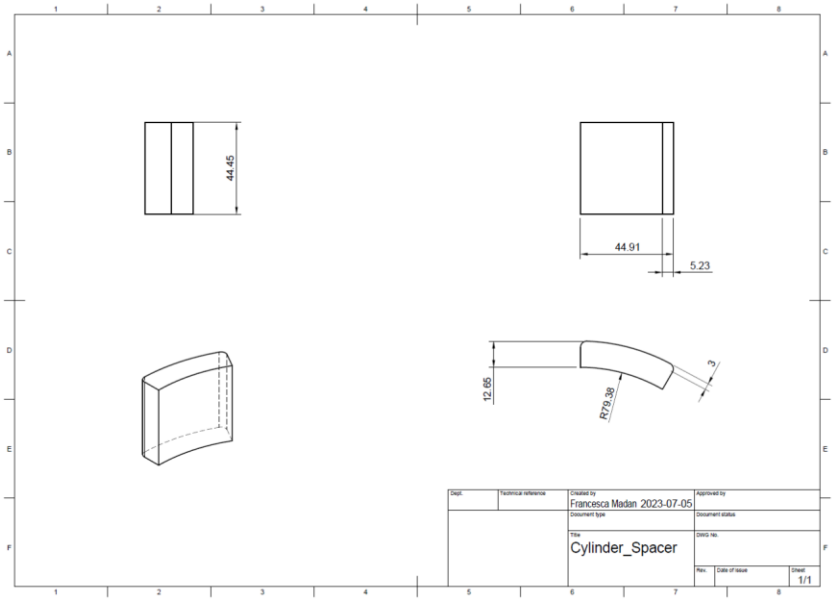

Figure 48. Manufacturing 2D-drawing for spacers on the current charge measurement container used to attach clasps.

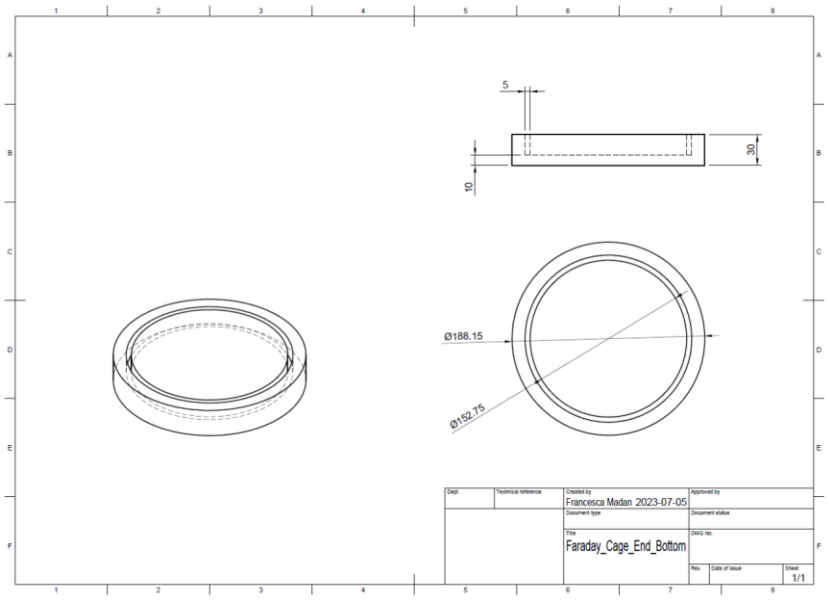

Figure 49. Manufacturing 2D-drawing for the bottom of the charge measurement container in design 2 holding the Faraday Cup.

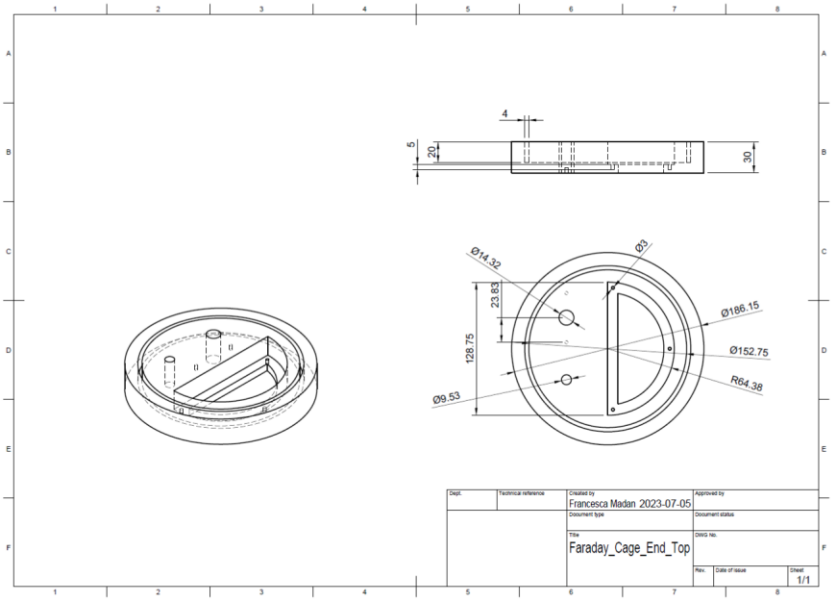

Figure 50. Manufacturing 2D-drawing for the top of the charge measurement container in design 2 holding the Faraday Cup.

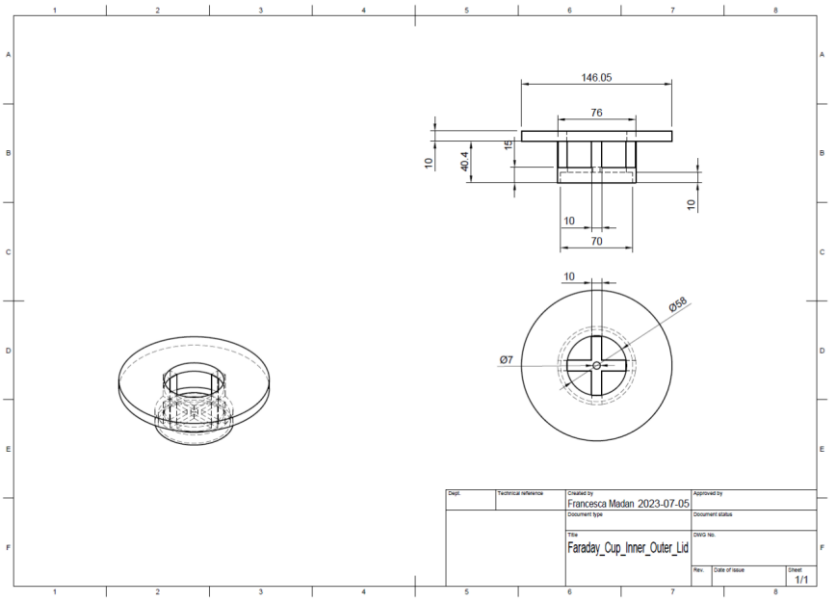

Figure 51. Manufacturing 2D-drawing for lid used on Faraday cup for charge measurement design 1 and 2.

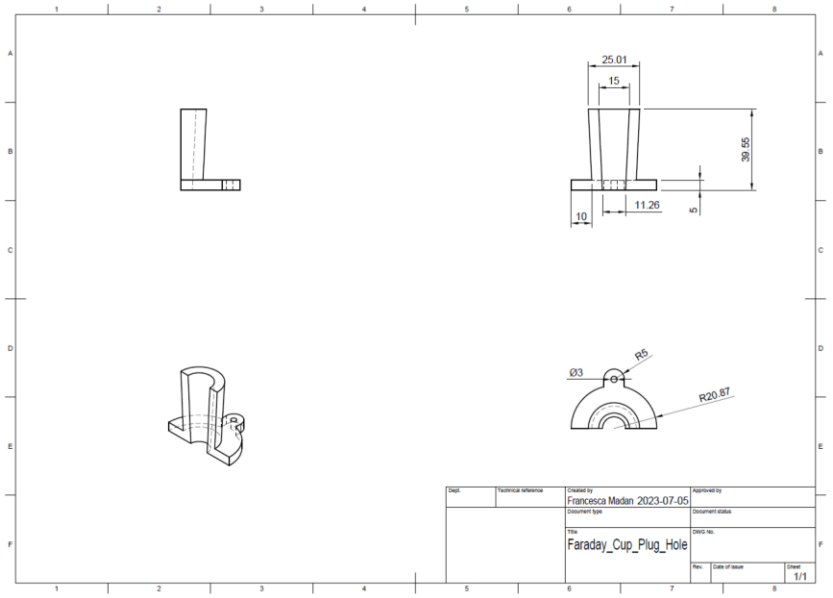

Figure 52. Manufacturing 2D-drawing for addition to figure 31's container top used to allow access to the cable connected to the Faraday Cup.

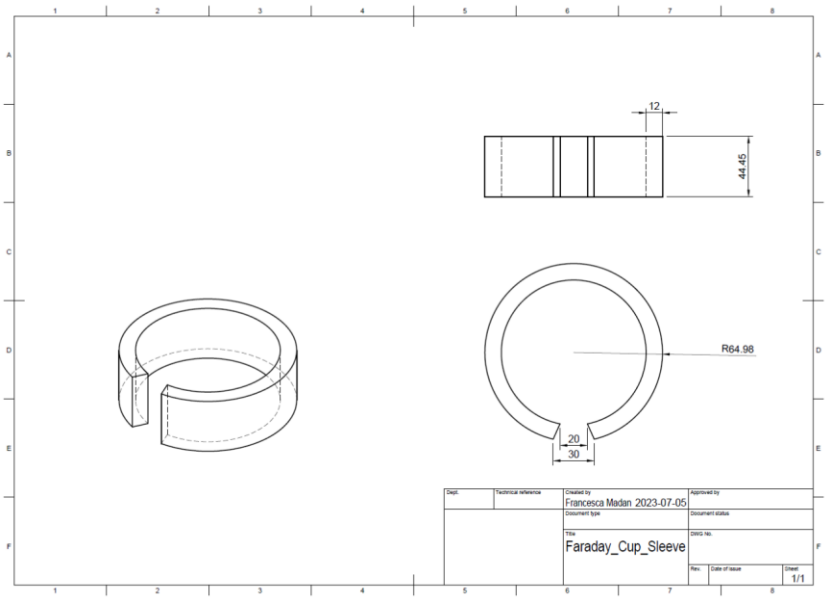

Figure 53. Manufacturing 2D-drawing for a sleeve used to provide an airtight seal to the Faraday Cup lid shown in figure 32. This is used in tandem with figure 34, spacers connected to the sleeve.

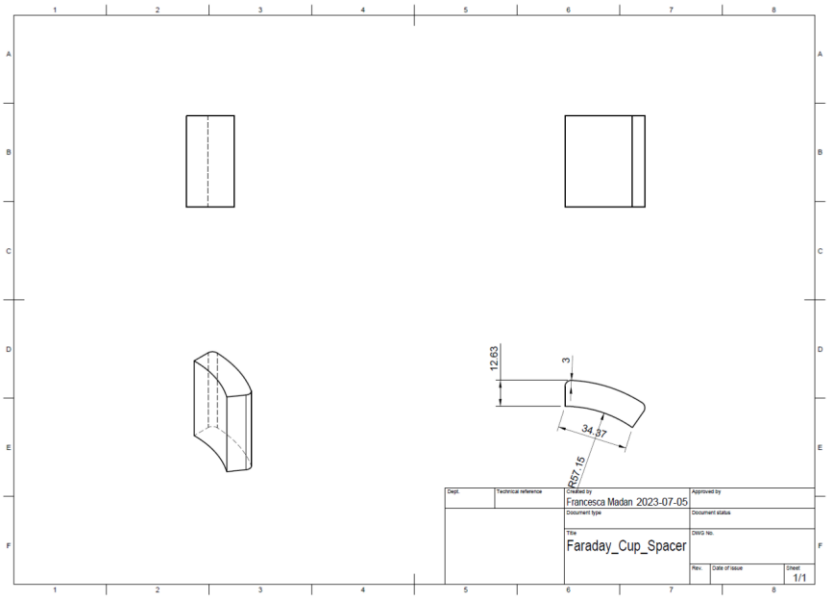

Figure 54. Manufacturing 2D-drawing for spacers attached to faraday sleeve (figure 33). Used to provide airtight seal to Faraday Cup and Faraday Cup lid (figure 32).

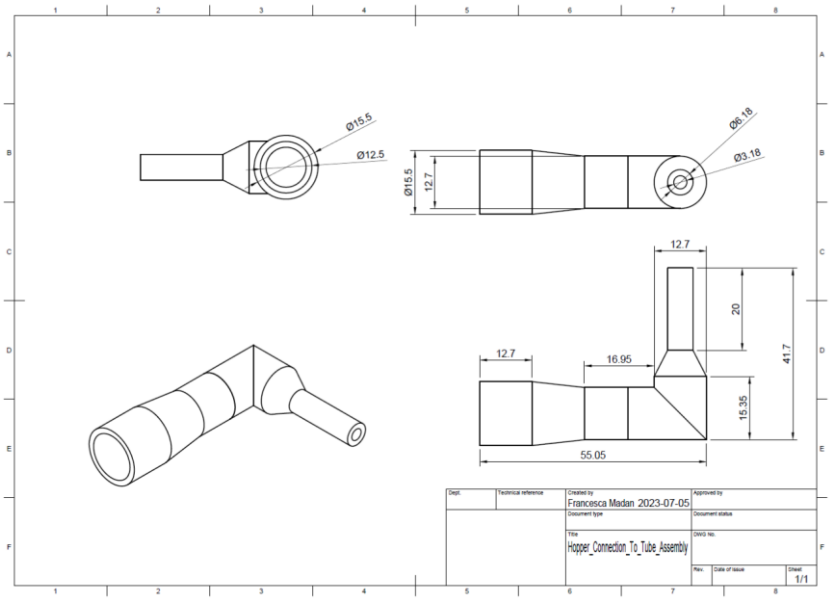

Figure 55. Manufacturing 2D-drawing for connection for hopper to tube used in mass delivery design 3.

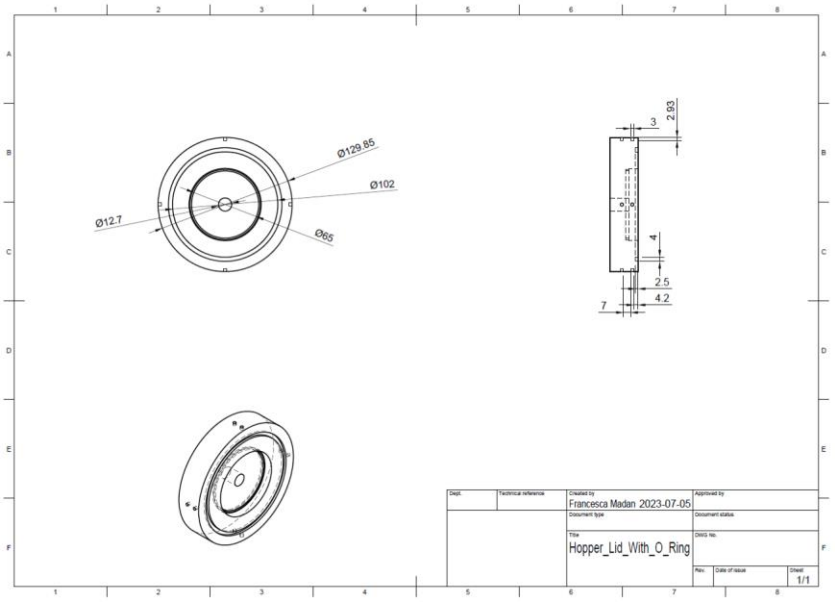

Figure 56. Manufacturing 2D-drawing for hopper lid with connection to airflow used in all mass delivery designs. The addition of the O-ring cutout was only inputted in design 3.

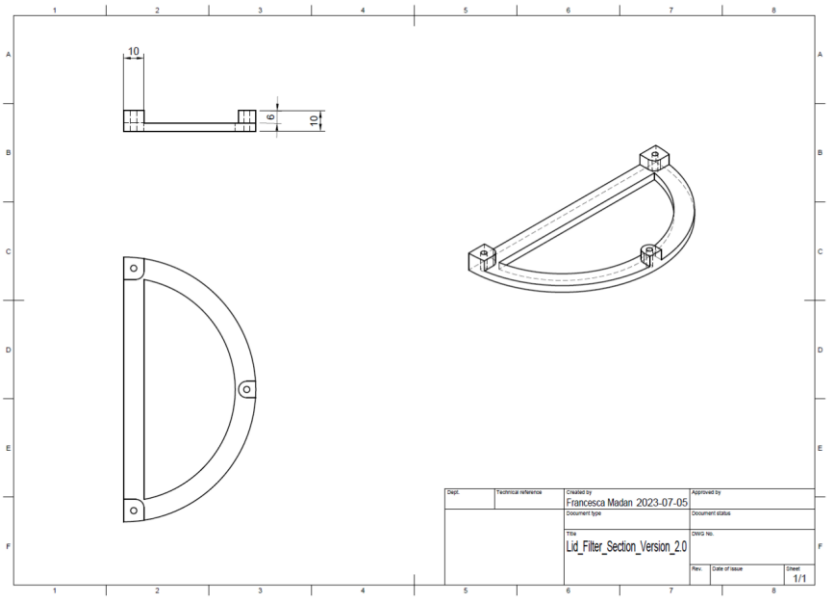

Figure 57. Manufacturing 2D-drawing for filter lid used on the top of the mass delivery container lid (figure 31). Used to allow air to escape the container.

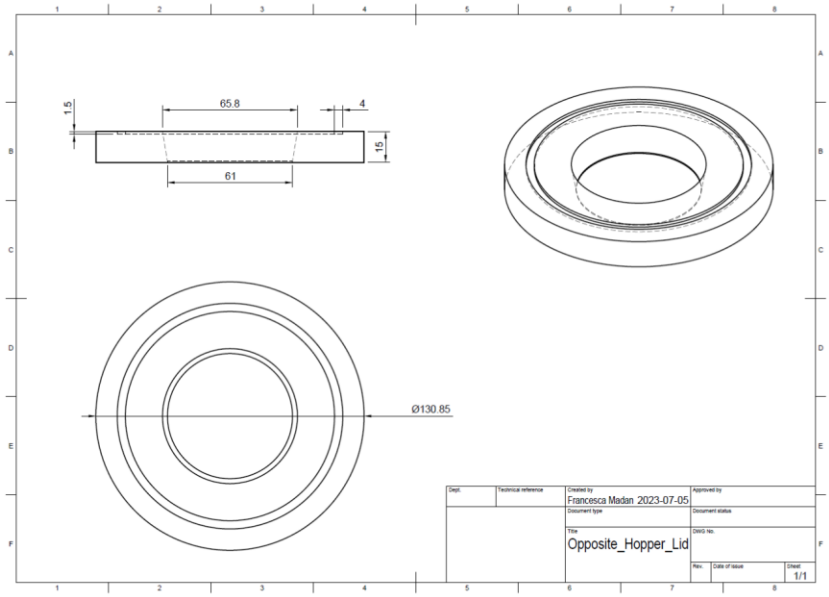

Figure 58. Manufacturing 2D-drawing for opposite side of the hopper lid (figure 37), used to provide an airtight seal. This was designed for mass delivery system 3.

References

Telko, M. J., Kujanpää, J., & Hickey, A. J. (2007). Investigation of triboelectric charging in dry powder inhalers using electrical low pressure impactor (ELPI™). *International journal of pharmaceutics*, *336*(2), 352-360.

Chen, Y., Young, P. M., Fletcher, D. F., Chan, H. K., Long, E., Lewis, D., ... & Traini, D. (2015). The effect of actuator nozzle designs on the electrostatic charge generated in pressurised metered dose inhaler aerosols. *Pharmaceutical research*, *32*(4), 1237-1248.

Wang, H., Fotovat, F., Bi, X. T., & Grace, J. R. (2019). Tribo-charging of binary mixtures composed of coarse and fine particles in gas–solid pipe flow. *Particuology*, *43*, 101-109.

Assatory, A., Vitelli, M., Rajabzadeh, A. R., & Legge, R. L. (2019). Dry fractionation methods for plant protein, starch and fiber enrichment: A review. Trends in Food Science & Technology, 86, 340–351. https://doi.org/10.1016/j.tifs.2019.02.006

Karner, S., & Urbanetz, N. A. (2013). Triboelectric characteristics of mannitol based formulations for the application in dry powder inhalers. *Powder technology*, *235*, 349-358.

Karner, S., Maier, M., Littringer, E., & Urbanetz, N. A. (2014). Surface roughness effects on the tribo-charging and mixing homogeneity of adhesive mixtures used in dry powder inhalers. *Powder technology*, *264*, 544-549.

Zafar, U., Alfano, F., & Ghadiri, M. (2018). Evaluation of a new dispersion technique for assessing triboelectric charging of powders. *International journal of pharmaceutics*, *543*(1-2), 151-159.

Pierson, J. (n.d.). The espart analyzer uses the principle of stokes' law and laser Doppler effect in determining the particle size and charge. as. - ppt download. SlidePlayer. https://slideplayer.com/slide/4851854/

Mehrtash, H. (2021). A triboelectric-based method for rapid characterization of powders.

Németh, E., Albrecht, V., Schubert, G., & Simon, F. (2003). Polymer tribo-electric charging: dependence on thermodynamic surface properties and relative humidity. *Journal of Electrostatics*, *58*(1-2), 3-16.

Schwindt, N., von Pidoll, U., Markus, D., Klausmeyer, U., Papalexandris, M. V., & Grosshans, H. (2017). Measurement of electrostatic charging during pneumatic conveying of powders. *Journal of Loss Prevention in the Process Industries*, *49*, 461-471.

Taghavivand, M. (2021). *Role of Catalyst Support and Continuity Additives on the Degree of Electrostatic Charging and Reactor Fouling in Polyethylene Gas-solid Fluidized Bed Reactors* (Doctoral dissertation, Université d'Ottawa/University of Ottawa).

Trigwell, S., Grable, N., Yurteri, C. U., Sharma, R., & Mazumder, M. K. (2003). Effects of surface properties on the tribocharging characteristics of polymer powder as applied to industrial processes. *IEEE Transactions on Industry Applications*, *39*(1), 79-86.

Matsusaka, Shuji, et al. "Triboelectric charging of powders: A review." *Chemical Engineering Science* 65.22 (2010): 5781-5807.

Zhang, Guangwen, et al. "Effect of tribocharger material on the triboelectric characteristics of coal and mineral particles." *Particulate Science and Technology* 35.5 (2017): 583-588.

Krämer, H. "Safety aspects of electrostatic paint, powder and flock spraying processes." *Journal of Electrostatics* 30 (1993): 77-92.

Jocham, C., Schmidt, T. W., Wuzella, G., Teischinger, A., & Kandelbauer, A. (2011). Adhesion improvement of powder coating on medium density fibreboard (MDF) by thermal pre-treatment. *Journal of Adhesion Science and Technology*, *25*(15), 1937-1946.

Kramer, H. "Recent developments in the safety consideration of electrostatic spraying processes." *Particulate science and technology* 16.1 (1998): 69-76.

Krämer, H. (1993). Safety aspects of electrostatic paint, powder and flock spraying processes. *Journal of Electrostatics*, *30*, 77-92.

Lee, L. H. (1994). Dual mechanism for metal-polymer contact electrification. *Journal of electrostatics*, *32*(1), 1-29.

Mizes, H. A., Conwell, E. M., & Salamida, D. P. (1990). Direct observation of ion transfer in contact charging between a metal and a polymer. *Applied physics letters*, *56*(16), 1597-1599.

Saurenbach, F., Wollmann, D., Terris, B. D., & Diaz, A. F. (1992). Force microscopy of ion-containing polymer surfaces: morphology and charge structure. *Langmuir*, *8*(4), 1199-1203.

Tanoue, K. I., Ema, A., & Masuda, H. (1999). Effect of material transfer and work hardening of metal surface on the current generated by impact of particles. *Journal of chemical engineering of Japan*, *32*(4), 544-548.

Harper, W. R. (1951). The Volta effect as a cause of static electrification. *Proceedings of the Royal Society of London. Series A. Mathematical and Physical Sciences*, *205*(1080), 83-103.

Moughrabiah, W. O., Grace, J. R., & Bi, X. T. (2009). Effects of pressure, temperature, and gas velocity on electrostatics in gas− solid fluidized beds. *Industrial & Engineering Chemistry Research*, *48*(1), 320-325.

Yang, W. C. (1998). *Fluidization, Solids Handling, and Processing: Industrial Applications*. Elsevier.

Mehrani, P. (2005). *Characterization of electrostatic charges in gas-solid fluidized beds* (Doctoral dissertation, University of British Columbia).

Marjamäki, M., Keskinen, J., Chen, D. R., & Pui, D. Y. (2000). Performance evaluation of the electrical low-pressure impactor (ELPI). *Journal of Aerosol Science*, *31*(2), 249-261.

Landauer, Johann, et al. “Effect of Particle-Wall Interaction on Triboelectric Separation of Fine Particles in a Turbulent Flow.” Advanced Powder Technology : the International Journal of the Society of Powder Technology, Japan, vol. 30, no. 5, 2019, pp. 1099–107, https://doi.org/10.1016/j.apt.2019.03.006.

Karner, Stefan, et al. “Triboelectrics: The Influence of Particle Surface Roughness and Shape on Charge Acquisition During Aerosolization and the DPI Performance.” Powder Technology, vol. 262, 2014, pp. 22–29, https://doi.org/10.1016/j.powtec.2014.04.025.

Wang, Haifeng, et al. “Tribo-Charging of Binary Mixtures Composed of Coarse and Fine Particles in Gas–solid Pipe Flow.” Particuology, vol. 43, 2019, pp. 101–09, https://doi.org/10.1016/j.partic.2018.07.001.

Yanar, D. K., and B. A. Kwetkus. “Electrostatic Separation of Polymer Powders.” Journal of Electrostatics, vol. 35, no. 2, 1995, pp. 257–66, https://doi.org/10.1016/0304-3886(94)00044-W.

Albrecht, Victoria, et al. “Some Aspects of the Polymers’ Electrostatic Charging Effects.” Journal of Electrostatics, vol. 67, no. 1, 2009, pp. 7–11, https://doi.org/10.1016/j.elstat.2008.10.002.

Cruise, R. D., Hadler, K., Starr, S. O., & Cilliers, J. J. (2022). The effect of particle size and relative humidity on triboelectric charge saturation. Journal of Physics. D, Applied Physics, 55(18), 185306–. https://doi.org/10.1088/1361-6463/ac5081

Németh, Ernő, et al. “Polymer Tribo-Electric Charging: Dependence on Thermodynamic Surface Properties and Relative Humidity.” Journal of Electrostatics, vol. 58, no. 1, 2003, pp. 3–16, https://doi.org/10.1016/S0304-3886(02)00137-7.

Aríñez-Soriano, J., Albalad, J., Vila-Parrondo, C., Pérez-Carvajal, J., Rodríguez-Hermida, S., Cabeza, A., Juanhuix, J., Imaz, I., & Maspoch, D. (2016). Single-crystal and humidity-controlled powder diffraction study of the breathing effect in a metal-organic framework upon water adsorption/desorption. Chemical Communications (Cambridge, England), 52(45), 7229–7232. https://doi.org/10.1039/c6cc02908f

Xiaosong Ma, et al. “Characterization and Modeling of Moisture Absorption of Underfill for IC Packaging.” 2007 8th International Conference on Electronic Packaging Technology, IEEE, 2007, pp. 1–5, https://doi.org/10.1109/ICEPT.2007.4441451.

Marchetti, Lorenzo, et al. “Negative Impact of Humidity on the Flowability of Steel Powders.” Particulate Science and Technology, vol. 40, no. 6, 2022, pp. 722–36, https://doi.org/10.1080/02726351.2021.1995091.

Fayed, Muhammad E., and Thomas S. Skocir. “Screw Conveyors and Feeders.” Mechanical Conveyors, 1st ed., CRC Press, 1997, pp. 167–223, https://doi.org/10.1201/9780203747902-4.

Ali, Syed Sadiq, et al. “Effect of Modified Inlet Flow Strategy on the Segregation Phenomenon in Pulsed Fluidized Bed of Ultrafine Particles: A Collapse Bed Study.” Chemical Engineering and Processing, vol. 159, 2021, p. 108243–, https://doi.org/10.1016/j.cep.2020.108243.

Limtrakul, Sunun, et al. “Lagrangian Modeling and Simulation of Effect of Vibration on Cohesive Particle Movement in a Fluidized Bed.” Chemical Engineering Science, vol. 62, no. 1, 2007, pp. 232–45, https://doi.org/10.1016/j.ces.2006.08.020.

Järvinen, A., Aitomaa, M., Rostedt, A., Keskinen, J. & Yli-Ojanperä, J. 2014. Calibration of the new ELPI®+VI software can be used for instrument control electrical low pressure impactor (ELPI+). 2014 J. Aerosol Sci. 69, pp. 150-159.

Naik, S., Sarkar, S., Gupta, V., Hancock, B. C., Abramov, Y., Yu, W., & Chaudhuri, B. (2015). A combined experimental and numerical approach to explore tribocharging of pharmaceutical excipients in a hopper chute assembly. *International Journal of Pharmaceutics*, *491*(1-2), 58–68. https://doi.org/10.1016/j.ijpharm.2015.05.081

Sippola, P., Kolehmainen, J., Ozel, A., Liu, X., Saarenrinne, P., & Sundaresan, S. (2018). Experimental and numerical study of wall layer development in a tribocharged fluidized bed. *Journal of Fluid Mechanics, 849*, 860-884. doi:10.1017/jfm.2018.412

Nomura, T., Satoh, T., & Masuda, H. (2003). The environment humidity effect on the tribo-charge of powder. *Powder Technology*, *135*(1), 43–49. https://doi.org/10.1016/S0032-5910(03)00157-8

Mehrani, P., Bi, H. T., & Grace, J. R. (2007). Electrostatic behavior of different fines added to a Faraday cup fluidized bed. Journal of Electrostatics, 65(1), 1–10. https://doi.org/10.1016/j.elstat.2006.05.002

Jamie Clayton,Chapter 17 - An Introduction to Powder Characterization,Editor(s): Ajit S. Narang, Sherif I.F. Badawy,Handbook of Pharmaceutical Wet Granulation,Academic Press,2019, Pages 569-613, ISBN 9780128104606, https://doi.org/10.1016/B978-0-12-810460-6.00021-X.

Marefatallah, Maedeh. "Study of Local Solid Volume Fraction Fluctuations in a Liquid Fluidized Bed." *University of Alberta*, 2019, pp. 15–16.

Galayko, D., Dudka, A., Karami, A., O'Riordan, E., Blokhina, E., Feely, O., & Basset, P. (2015). Capacitive Energy Conversion With Circuits Implementing a Rectangular Charge-Voltage Cycle-Part 1: Analysis of the Electrical Domain. IEEE Transactions on Circuits and Systems. I, Regular Papers, 62(11), 2652–2663. https://doi.org/10.1109/TCSI.2015.2451911

Mirkowska, M., Kratzer, M., Teichert, C., & Flachberger, H. (2016). Principal Factors of Contact Charging of Minerals for a Successful Triboelectrostatic Separation Process – a Review. BHM. Berg- Und Hüttenmännische Monatshefte, 161(8), 359–382. https://doi.org/10.1007/s00501-016-0515-1

Kolehmainen, J., Sippola, P., Raitanen, O., Ozel, A., Boyce, C. M., Saarenrinne, P., & Sundaresan, S. (2017). Effect of humidity on triboelectric charging in a vertically vibrated granular bed: Experiments and modeling. Chemical Engineering Science, 173(C), 363–373. https://doi.org/10.1016/j.ces.2017.08.006

Rezende, C. A., Gouveia, R. F., da Silva, M. A., & Galembeck, F. (2009). Detection of charge distributions in insulator surfaces. Journal of Physics: Condensed Matter, 21(26). https://doi.org/10.1088/0953-8984/21/26/263002

Biegaj, K.W., Rowland, M., Lukas, T.M., & Heng, J.Y. (2017). Surface Chemistry and Humidity in Powder Electrostatics: A Comparative Study between Tribocharging and Corona Discharge. *ACS Omega, 2*, 1576 - 1582.

Badawy, S. I. F., & Narang, A. S. (2019). *Handbook of pharmaceutical wet granulation : theory and practice in a quality by design paradigm*. Academic Press is an imprint of Elsevier.

Anderson, J. H., & Fox, E. (1995). Tribocharging of Three-Component Powder Mixtures. The Journal of Adhesion, 51(1-4), 27–40. https://doi.org/10.1080/00218469508009987

Samira. (2021, March 23). *How to make chickpea flour (two methods!)*. Alphafoodie. https://www.alphafoodie.com/how-to-make-chickpea-flour/

ASM Handbook, Volume 7: Powder Metal Technologies and Applications P.W. Lee, Y. Trudel, R. Iacocca, R.M. German, B.L. Ferguson, W.B. Eisen, K. Moyer, D. Madan, and H. Sanderow, editors, p 287-301 DOI: 10.1361/asmhba0001530

Trigwell, S., Mazumder, M. K., & Pellissier, R. (2001). Tribocharging in electrostatic beneficiation of coal: Effects of surface composition on work function as measured by x-ray photoelectron spectroscopy and ultraviolet photoelectron spectroscopy in air. Journal of Vacuum Science & Technology A: Vacuum, Surfaces, and Films, 19(4), 1454–1459. https://doi.org/10.1116/1.1379320

Matsuyama T. and Yamamoto H., (1994). "Charge transfer between a polymer particle and a metal plate due to impact," in *IEEE Transactions on Industry Applications*, vol. 30, no. 3, pp. 602-607, doi: 10.1109/28.293706.

Liu, X., Kolehmainen, J., Nwogbaga, I., Ozel, A., & Sundaresan, S. (2020). Effect of particle size on tribocharging. Powder Technology, 375, 199–209. https://doi.org/10.1016/j.powtec.2020.07.078

Landauer, Johann, and Petra Foerst. (2019). "Influence of Particle Contact Number on Triboelectric Separation Selectivity" *Processes* 7, no. 10: 716. https://doi.org/10.3390/pr7100716

Tabtabaei, S., Konakbayeva, D., Rajabzadeh, A. R., & Legge, R. L. (2019). Functional properties of navy bean (Phaseolus vulgaris) protein concentrates obtained by pneumatic tribo-electrostatic separation. Food Chemistry, 283, 101–110. https://doi.org/10.1016/j.foodchem.2019.01.031

Hakim, L. F., Portman, J. L., Casper, M. D., & Weimer, A. W. (2005). Aggregation behavior of nanoparticles in fluidized beds. Powder Technology, 160(3), 149–160. https://doi.org/10.1016/j.powtec.2005.08.019

Rezaei, H., Lim, C. J., Lau, A., & Sokhansanj, S. (2016). Size, shape and flow characterization of ground wood chip and ground wood pellet particles. Powder Technology, 301(C), 737–746. https://doi.org/10.1016/j.powtec.2016.07.016